Impacts of urbanization on air quality and related health risks in a city with complex terrain

Chenchao Zhan [a, b], Min Xie [a,*], Hua Lu [c], Bojun Liu [d], Zheng Wu [c], Tijian Wang [a], Bingliang Zhuang [a], Mengmeng Li [a], Shu Li [a]

[a] School of Atmospheric Sciences, Nanjing University, Nanjing 210023, China

[b] School of Atmospheric Physics, Nanjing University of Information Science and Technology, Nanjing 210044, China

[c] Chongqing Institute of Meteorological Sciences, Chongqing 401147, China

[d] Chongqing Meteorological Observatory, Chongqing 401147, China

----

[*] Corresponding author. minxie@nju.edu.cn (M. Xie)

Abstract: Urbanization affects air pollutants via urban expansion and emission growth, and thereby inevitably changes the health risks of air pollutants. However, the health risks related to urbanization are rarely estimated, especially for cities with complex terrain. In this study, a highly urbanized city with severe air pollution and complex terrain (Chengdu) is selected to explore this issue. The effects of urban expansion are further compared with emission growth since air quality management is usually achieved by regulating anthropogenic emissions. Air pollution in Chengdu was mainly caused by $PM_{2.5}$ and O_3 from 2015 to 2021. $PM_{2.5}$ pollution tended to appear in cold months (November to February) owing to the blocking of air and the stable atmospheric layer, while O_3 pollution was likely to occur in warm months (April to August) because of the high temperature and strong sunlight dominated by high-pressure systems. From 2015 to 2021, the 7-year annual averages of premature mortalities from all non-accidental causes (ANAC) due to $PM_{2.5}$ and O_3 were 9386 [95% confidence intervals (CI): 6542–11726] and 8506 (95%CI: 4817–11882), respectively. Based on the characteristics of $PM_{2.5}$ and O_3, six numerical experiments were conducted to investigate the impacts of urban expansion and emission growth on health risks of air pollutants. The results show that urban land use led to an increase in air temperature and the boundary layer height compared to cropland, which was conducive to the diffusion of $PM_{2.5}$. Thus, the monthly average surface $PM_{2.5}$ concentrations decreased by 10.8 μg m^{-3} (7.6%) in January. However, the monthly average daily

maximum 8 h average (MDA8) O_3 concentrations increased by 10.6 μg m^{-3} (6.0%) in July owing to the stronger photochemical production and better vertical mixing during daytime. In this case, premature mortalities from ANAC due to $PM_{2.5}$ decreased by 171 (95%CI: 129–200, or about 6.9%) in January, and those due to O_3 increased by 203 (95%CI: 122–268, or about 9.5%) in July. As for the effects of emission growth, the monthly average $PM_{2.5}$ and MDA8 O_3 concentrations increased by 23.9 μg m^{-3} (16.8%) and 4.8 μg m^{-3} (2.7%) when anthropogenic emissions were taken into account. Premature mortalities from ANAC due to $PM_{2.5}$ and O_3 then increased by 388 (95%CI: 291–456, or about 15.7%) and 87 (95%CI: 54–112, or about 4.1%), respectively. From a health risk perspective, the effects of urban land use on health risks of $PM_{2.5}$ are about half that of anthropogenic emissions, whereas the effects of urban land use on health risks of O_3 can be 2 times that of anthropogenic emissions. This reminds us that, in addition to regulating anthropogenic emissions, urban planning is also important for urban air quality, especially for secondary pollutants like O_3.

Key Words: urbanization; land use; anthropogenic emissions; air quality; health risk;

1 Introduction

Air pollutants are substances that damage humans, plants and animals drastically when present in the atmosphere in sufficient concentration (Baklanov et al., 2016; Kinney, 2018; Pautasso et al., 2010). The most common air pollutants are ozone (O_3), fine particulate matter ($PM_{2.5}$, particulate matter with an aerodynamic diameter of 2.5 μm or less), sulfur dioxide (SO_2) and nitrogen oxides (NO_x, which is NO + NO_2). These air pollutants threaten human health in many parts of the world, evoking a series of health risks including cardiovascular diseases, respiratory diseases and chronic obstructive pulmonary disease (Brauer et al., 2016; Lelieveld et al., 2013; Manisalidis et al., 2020). According to the World Health Organization (WHO), exposure to ambient air pollutants is associated with 4.2 million premature deaths worldwide annually (https://www.who.int/health-topics/air-pollution#tab=tab_2).

Most of those premature deaths occur in urban areas as urban areas currently host more than 50% of the population (over 3.5 billion people). This proportion is projected to increase to 70% by 2050 due to ongoing urbanization (UNDESA, 2018). Urbanization since the industrial revolution in the 19th century has led to a profound modification of land use via urban expansion (Seto et al., 2012). Natural surfaces are replaced by impervious surfaces, then the surface physical properties (e.g.., albedo, thermal inertia and roughness) and processes (e.g., the exchange of water, momentum and energy) are modified. These changes in surface physical properties and processes exert an important influence on urban meteorology and air quality, which has been widely acknowledged in previous studies. Wang et al. (2009) explored the impacts of urban expansion on weather conditions and its implication on O_3 concentration in the Pearl River Delta, and pointed out that urban land use changes can cause an increase in 2-m temperature by 1.0%–3.7%, an increase in planetary boundary layer height by 5.9%–6.3% and an increase in surface O_3 concentration by 4.2%–8.5%. Liao et al. (2015) conducted a similar study in the Yangtze River Delta, and found that urbanization increased 2-m temperature, planetary boundary layer and surface O_3 concentration but decreased surface PM_{10} (particulate matter with an aerodynamic diameter of 10 μm or less) concentration. Similar conclusions about the impacts of urbanization on meteorology and air quality have also been reported in the Beijing-Tianjin-Hebei region (Yu et al., 2012) and the Sichuan Basin (Wang et al., 2021, 2022a).

Urban areas are centers of resource utilization and are a major contributor to air pollutants and greenhouse gas emissions (Karl et al., 2019; Qian et al., 2022). According to the UN-Habitat (https://unhabitat.org/topic/energy), cities consume about 75% of global primary energy and emit 50%–60% of the world’s total greenhouse gases. Air pollutants that originate from anthropogenic sources can accumulate and degrade urban air quality under unfavorable meteorological conditions characterized by weak winds, which leaves urban dwellers vulnerable to air pollution (Holman et al., 2015; Lin and Zhu, 2018). Excessive emissions are the root cause of poor air quality in urban areas, and thereby efforts have been made to reduce anthropogenic emissions to achieve the goal of urban air pollution control. Urbanization can increase urban land use and anthropogenic emissions, which will affect the concentrations as well as health risks of air pollutants. However, the health risks related to urbanization are rarely estimated, especially for those cities with complex terrain. This is of great concern to policymakers and can inspire future air quality control strategies.

Although building in the mountains is not as easy as in the plains, about 12% of the global population (over 720 million people) resides in mountainous areas for historical, political, strategic and economic reasons. It is thus important to understand the fate of air pollutants in mountainous cities, where air pollution is usually more severe than in flat locations as the atmospheric dispersion is limited in mountainous areas (Zardi and Whiteman, 2013). The mountain-plain wind, resulting from horizontal temperature differences between air over mountain massifs and the air over the surrounding plains, is a key feature of the climatology of mountainous regions (Whiteman, 2000), which is important in determining the transport and dispersion of air pollutants. During daytime, the plain-to-mountain wind (plain wind) brings low-level air into the mountain massifs, whereas the mountain-to-plain wind (mountain wind) brings air out of the mountain massifs during nighttime. This wind system can often recirculate urban air pollutants and worsen air quality. Examples can be found in Mexico City (Molina et al., 2010), Hong Kong (Guo et al., 2013), Seoul (Ryu et al., 2013), the Salt Lake Valley (Baasandorj et al., 2017), the Colorado Front Range (Bahreini et al., 2018), the Alps (Karl et al., 2019) and the Taiwan Island (Lee et al., 2019).

Chengdu (104.01°E, 30.70°N) is the largest city in western China, occupying an area of 12,390 square kilometers with a population of more than 20 million. Located in the west of the Sichuan Basin, this city is surrounded by the Tibetan Plateau to the west, the Wu Mountains to the east, the Yunnan-Guizhou Plateau to the south and the Daba Mountains to the north (Figure 1a). Chengdu has experienced rapid urbanization over the past few decades with a surge in urban construction lands and a loss of cropland (Dai et al., 2021; Figure 1b). Luo et al. (2021) reported that Chengdu's urban area has increased by four times from 1996 to 2016. Because of the substantial anthropogenic emissions from human activities and the poor atmospheric diffusion capacity associated with terrain, Chengdu is one of the most polluted cities in China and has suffered from severe $PM_{2.5}$ and O_3 pollution in recent years (Shu et al., 2021; Yang et al., 2020; Zhan et al., 2019). Complex terrain, rapid urbanization and severe air pollution make Chengdu an ideal place to study the impact of urbanization on health risks of air pollutants in mountainous areas. The results could also provide valuable insight for other cities with complex terrain in the world.

In this study, we investigate the impacts of urbanization on air pollutant concentrations and the corresponding health risks in Chengdu. We also compare the impacts of urban expansion with emission growth. First, the basic characteristics of air pollutants in Chengdu from 2015 to 2021 are analyzed. Then, the impacts of urbanization on air pollutant concentrations are investigated using the WRF-Chem model. Finally, premature mortalities attributable to changes in air pollutant concentrations are estimated using the standard damage function. The rest of this paper is organized as follows. Section 2 introduces the data, the model configurations and the experimental designs.

Section 3 shows the main results and discussions. The conclusions are given in Section 4.

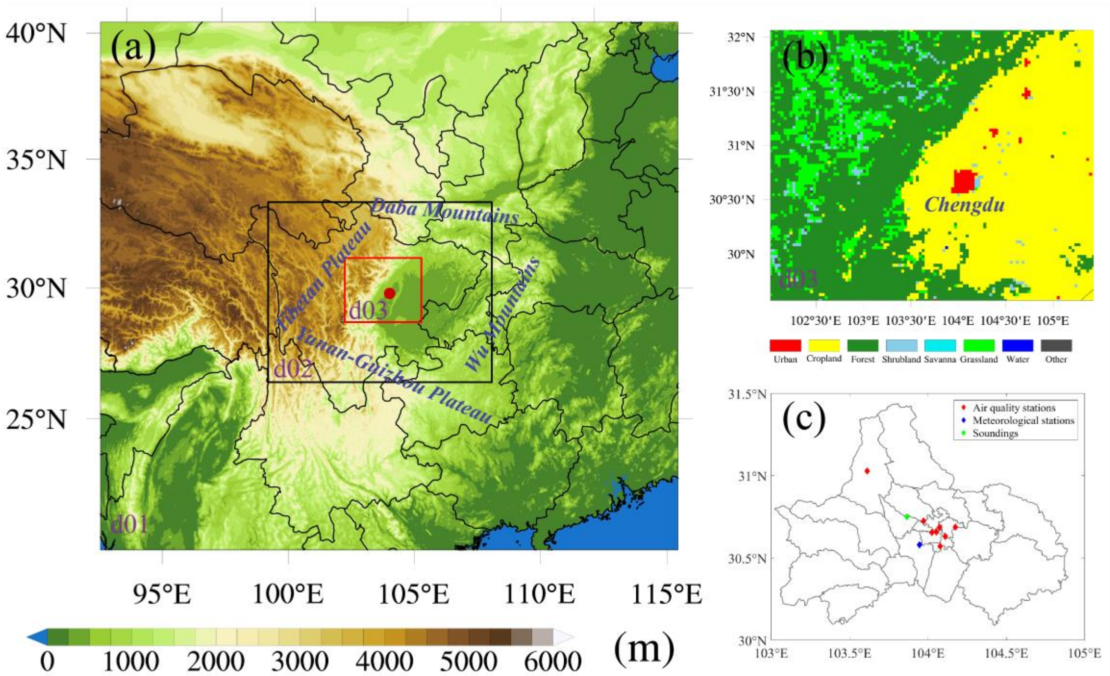

Figure 1. (a) Map of three nested WRF-Chem domains with terrain heights, (b) domain 3 with land cover maps and (c) locations of air quality stations, meteorological stations and soundings in Chengdu. The red dot in (a) shows the location of Chengdu.

2 Data and methods

2.1 Air quality and meteorological data

Air pollutants, including $PM_{2.5}$, PM_{10}, O_3, NO_2, SO_2 and CO, are monitored by the National Environmental Monitoring Center of China. These data are hourly issued on the national urban air quality real-time publishing platform (http://106.37.208.233:20035/). The monitoring data are strictly in accordance with the national monitoring regulations (http://www.cnemc.cn/jcgf/dqhj/). It should be noted that the O_3 measurements are reported in the unit of μg m^{-3} at the standard atmospheric conditions (273.15 K, 1 atm) before September 2018, and at 298.15 K conditions afterward. There are eight air quality stations throughout Chengdu (Figure 1c), and the urban hourly pollutant concentrations reported in this paper are the average results of measurements at all monitoring sites. The daily $PM_{2.5}$ concentrations are obtained by averaging observations over 24 hours of the day. The daily maximum 8 h average (MDA8) O_3 concentrations are calculated only on days with more than 18 h of O_3 measurements.

Surface meteorological data, including 2-m air temperature (T_2), 2-m dew point temperature (TD_2), 10-m wind speed (WS_{10}) and 10-m wind direction (WD_{10}), are taken from the website of the University of Wyoming at station ZUUU (http://weather.uwyo.edu/surface/). To verify upper-air fields, the sounding observations at Wenjiang (station 56187) are also acquired from this website. These sounding data contain temperature, dew point temperature and wind speed, etc. at different pressure layers with a time resolution of 12 h (00:00 and 12:00 UTC), and are often plotted on a Skew-T diagram (https://www.ncl.ucar.edu/Applications/skewt.shtml#ex2).

2.2 WRF-Chem model and experimental designs

WRF-Chem is the Weather Research and Forecasting (WRF) model coupled with Chemistry, in which meteorological and chemical variables use the same coordinates, transport schemes and physics schemes in space and time (Grell et al., 2005). WRF-Chem version 3.9.1 is employed in this study. As shown in Figure 1a, three nested domains are used with the grid spacing of 27, 9 and 3 km, respectively. 32 sigma levels are extending from the surface to 100 hPa in the vertical direction with 12 levels located below 2 km to resolve the boundary layer processes. The height of the lowest model level is about 25 m. The MODIS-based land use data set as default in WRF are selected. The domains and main options for physical and chemical parameterization schemes are listed in Table 1. The National Centers for Environmental Prediction (NCEP) Final (FNL) reanalysis data with a resolution of 1° × 1° at 6 h time intervals are adopted as the initial and boundary conditions for meteorological fields. Anthropogenic emissions are provided by the Multi-resolution Emission Inventory for China (MEIC) with a grid resolution of 0.25° × 0.25°. It should be noted that we empirically cut the $PM_{2.5}$ emissions by about 20% to avoid overestimation of $PM_{2.5}$ in the model. Biogenic emissions are calculated online using the Guenther scheme (Guenther et al., 2006).

Table 1. The domains and main options for WRF-Chem.

Items	Contents
Domains (x, y)	(94, 86), (109, 88), (112, 94)
Grid spacing (km)	27, 9, 3
Center	(104°E, 31°N)

Time step (s)	90
Microphysics	Purdue Lin scheme (Chen and Sun, 2002)
Longwave radiation	RRTM scheme (Mlawer et al., 1997)
Shortwave radiation	Goddard shortwave scheme (Matsui et al., 2018)
Surface layer	Monin-Obukhov scheme (Janjic, 1994)
Land-surface layer	Unified Noah land-surface model (Tewari et al., 2014)
Planetary boundary layer	Mellor-Yamada-Janjic TKE scheme (Janjic, 1994)
Cumulus parameterization	Grell 3D ensemble scheme (Grell and Devenyi, 2002)
Gas-phase chemistry	RADM2 (Stockwell et al., 1990)
Photolysis scheme	Fast-J photolysis (Fast et al., 2006)
Aerosol module	MADE/SORGAM (Schell et al., 2001)

To estimate the impacts of urbanization, six numerical simulations are designed (Table 2). The year of the numerical simulations is 2017 since the MEIC emission inventory is currently updated to 2017. Taking into account the computational cost, January is the representative of cold months with frequent $PM_{2.5}$ pollution, while July is the representative of warm months with frequent O_3 pollution (Section 3.1). Jan_Base is a baseline simulation using the MODIS land use and the MEIC emission inventory over all three domains. The land cover maps in domain 3 are particularly shown in Figure 1b. Jan_noCD is a sensitivity simulation, in which the urban land use of Chengdu is replaced by cropland to examine the impacts of urban expansion. Jan_noEmi is another sensitivity simulation, in which the anthropogenic emissions in Chengdu are shut down to identify the impacts of emission growth. The above three numerical experiments use the same configurations (Table 1) running from 00:00 UTC December 28, 2016 to 00:00 UTC February 1, 2017 with the first 96 h as spin-up time. July_Base, July_noCD and July_noEmi are the same as Jan_Base, Jan_noCD and Jan_noEmi, but run from 00:00 UTC June 27 to 00:00 UTC August 1, 2017 with the first 96 h as spin-up time.

Table 2. Six numerical simulations are conducted in this study.

Scenarios	Description

Jan_Base	Baseline simulation in January
Jan_noCD	Replacing urban land use of Chengdu with cropland in January
Jan_noEmi	Shutting down anthropogenic emissions in Chengdu in January
July_Base	Baseline simulation in July
July_noCD	Replacing urban land use of Chengdu with cropland in July
July_noEmi	Shutting down anthropogenic emissions in Chengdu in July

2.3 Health risks estimation

Daily premature mortalities attributable to $PM_{2.5}$ and O_3 exposure from all non-accidental causes (ANAC), cardiovascular diseases (CVD), respiratory diseases (RD) and chronic obstructive pulmonary diseases (COPD) are estimated using the standard damage function (Anenberg et al., 2010; Zhan et al., 2021):

$$\Delta M = y_0\left(\frac{RR-1}{RR}\right)\mathrm{Pop}, \quad (4)$$

where ΔM is the daily premature mortality, y_0 is the daily baseline mortality rate, RR is the relative risk, $(RR-1)/RR$ is the attributable fraction, and Pop is the exposed population. RR is calculated as follows:

$$RR = \exp(\beta(\mathrm{C}-\mathrm{C}_0)), \quad (5)$$

where β is the concentration-response function that relates a unit change in air pollutant concentrations to a change in health endpoint incidence. In practice, β usually represents the percentage increase in daily mortality associated with a 10 μg m^{-3} increase in daily $PM_{2.5}$/MDA8 O_3 concentrations. C is the exposure concentration, which is the daily average concentration for $PM_{2.5}$ and the MDA8 O_3 concentration for O_3. C_0 is the threshold concentration. When C is not greater than C_0, the value of $C–C_0$ is 0.

In this study, C_0 is 10 μg m^{-3} for daily $PM_{2.5}$ (Song et al., 2015), and 75.2 μg m^{-3} for MDA8 O_3 (Liu et al., 2018). β and y_0 for ANAC, CVD, RD and COPD are summarized in Table 3 (Chen et al., 2017; Yin et al., 2017). The populations of Chengdu provided by the National Bureau of Statistics of China are 16.853 million, 18.582 million, 19.188 million, 19.183 million, 20.409 million, 20.947 million and 20.938 million from 2015 to 2021.

We first calculate the $PM_{2.5}$- and O_3-induced daily premature mortalities using the methods mentioned above, and then add up the daily premature mortalities for the whole year/month to get the total premature mortalities. Since the largest uncertainty among the factors that determine premature mortalities usually comes from β, premature mortalities are presented as means and 95% confidence intervals (CI) based on β at 95% CI in this study. In addition, it should be noted that we use the average air pollutant concentration at all monitoring sites to represent air pollutant concentration in Chengdu. Correspondingly, the total population of Chengdu is used as the exposed population. Thus, our results are for Chengdu as a whole and do not address the spatial distribution of premature mortalities.

Table 3. Daily β and y_0 values for ANAC, CVD, RD and COPD.

Disease	β^* for $PM_{2.5}$	β for MDA8 O_3	y_0
ANAC	0.22 (0.15, 0.28)	0.24 (0.13, 0.35)	1.687×10^{-5}
CVD	0.27 (0.18, 0.36)	0.27 (0.10, 0.44)	3.880×10^{-6}
RD	0.29 (0.17, 0.42)	0.18 (–0.11, 0.47)	1.841×10^{-6}
COPD	0.38 (0.23, 0.53)	0.20 (–0.13, 0.53)	1.623×10^{-6}

$^*\beta$ is expressed as the percentage increase (posterior mean and 95% confidence intervals) in daily mortality associated with a 10 μg m^{-3} increase in daily $PM_{2.5}$/MDA8 O_3 concentrations.

3 Results and discussions

3.1 $PM_{2.5}$ and O_3 pollution in Chengdu

According to Chinese ambient air quality standards, $PM_{2.5}$ pollution occurs when daily $PM_{2.5}$ concentrations are greater than 75 μg m^{-3}, and O_3 pollution occurs when MDA8 O_3 concentrations are greater than 160 μg m^{-3}. As shown in Figure 2, Chengdu is suffering from severe $PM_{2.5}$ and O_3 pollution in recent years. There were 97, 101, 68, 53, 33, 43 and 37 $PM_{2.5}$ pollution episodes, and 61, 48, 42, 40, 42, 71 and 48 O_3 pollution episodes in Chengdu from 2015 to 2021. In China, the annual evaluation criterion for $PM_{2.5}$ is the annual average concentration, and for O_3 it is the 90th percentile of MDA8 O_3 concentration. The annual average concentrations of $PM_{2.5}$ were 60.7, 59.9, 52.6, 47.2, 40.6, 40.8 and 40.1 μg m^{-3}, and the 90th percentile of MDA8 O_3 concentrations were 183.0, 167.0, 168.0, 164.0, 171.5, 188.9 and 167.1 μg m^{-3} in Chengdu from 2015 to 2021. This suggests that $PM_{2.5}$ pollution improved significantly while O_3 pollution did not. O_3 pollution control in Chengdu should be taken seriously in the future. In addition, $PM_{2.5}$ and O_3 pollution had clear seasonal preferences, that is, $PM_{2.5}$ pollution tended to appear in cold months (November to February) while O_3 pollution preferred to appear in warm months (April to August). High $PM_{2.5}$ concentrations in cold months may be associated with the consumption of fossil fuels for heating and frequent temperature inversion. The high temperature and strong sunlight contribute to the elevated O_3 concentrations in warm months.

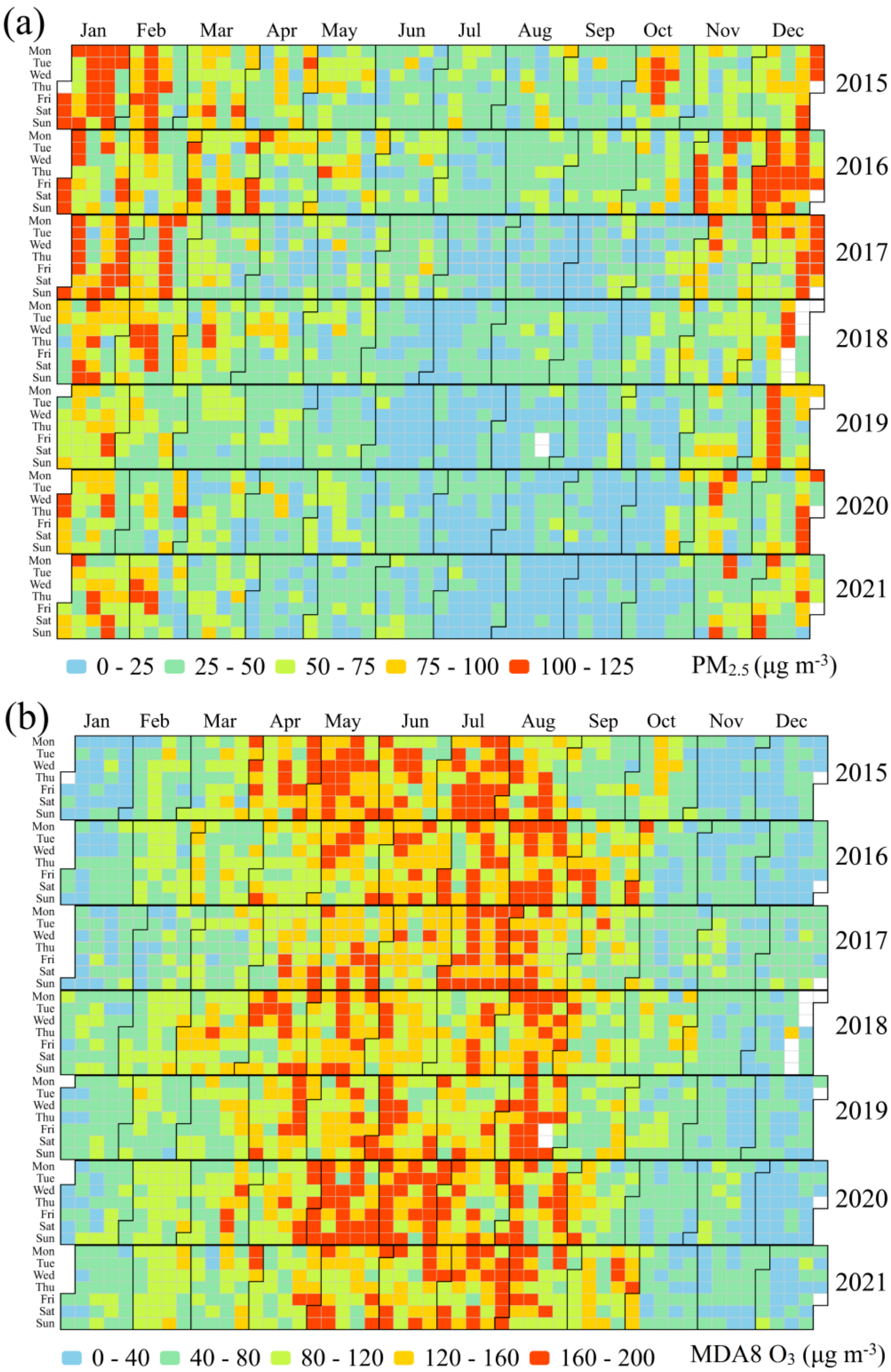

Figure 2. Heat maps of (a) daily $PM_{2.5}$ and (b) MDA8 O_3 concentrations in Chengdu from 2015 to 2021.

3.2 Premature mortality attributable to $PM_{2.5}$ and O_3

Severe $PM_{2.5}$ and O_3 pollution are responsible for a large number of premature mortalities in Chengdu. From 2015 to 2021, the premature mortalities from ANAC due to $PM_{2.5}$ were 10596

(95%CI: 7420–13186), 11647 (95%CI: 8140–14518), 10154 (95%CI: 7116–12630), 8942 (95%CI: 6214–11198), 7992 (95%CI: 5540–10031), 8298 (95%CI: 5759–10402) and 8072 (95%CI: 5606–10115), with the 7-year annual average of 9386 (95%CI: 6542–11726). The highest health risk among the diseases was from CVD with a 7-year annual average of 2609 (95%CI: 1788–3384), followed by COPD with a 7-year annual average of 1485 (95%CI: 941–1983) and RD with a 7-year annual average of 1321 (95%CI: 804–1840). This was mainly associated with the daily baseline mortality rate of different diseases (Table 3). Although Chengdu's population has been increasing by 24.2% from 2015 to 2021, premature mortalities due to $PM_{2.5}$ have generally declined (Figure 3a) owing to reduced $PM_{2.5}$ concentrations in recent years (Section 3.1).

The premature mortalities from ANAC due to O_3 were 7657 (95%CI: 4345–10672), 8025 (95%CI: 4537–11227), 7870 (95%CI: 4451–11005), 8824 (95%CI: 4967–12397), 7919 (95%CI: 4483–11065), 10085 (95%CI: 5749–13999) and 9163 (95%CI: 5185–12809) from 2015 to 2021, with a 7-year annual average of 8506 (95%CI: 4817–11882), about 90% of that due to $PM_{2.5}$. Unlike the overall reduction in premature mortalities due to $PM_{2.5}$, the premature mortalities due to O_3 increased slightly (Figure 3a), further indicating the urgent need for powerful O_3 control strategies in Chengdu.

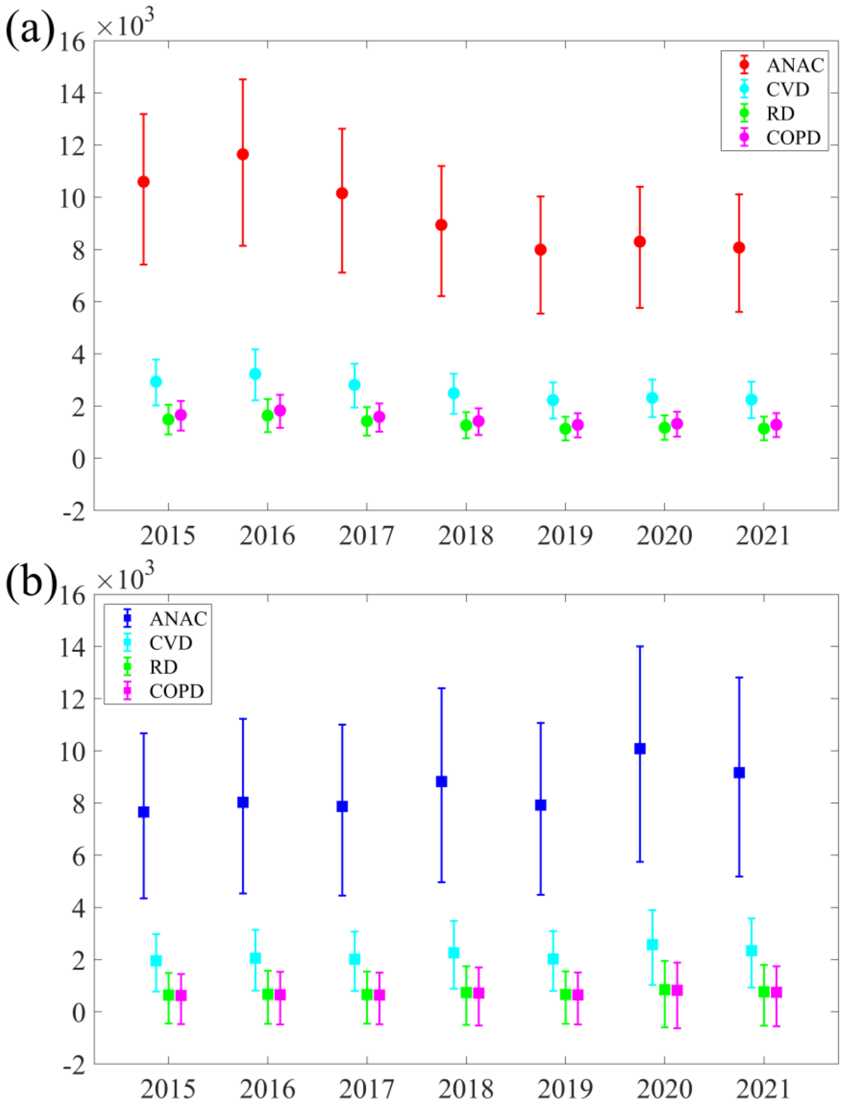

Figure 3. Premature mortality from ANAC, CVD, RD and COPD attributable to (a) $PM_{2.5}$ and (b) O_3 in Chengdu from 2015 to 2021. The dots represent the mean estimate, and the whiskers represent 95% confidence intervals.

3.3 Impacts of urbanization on $PM_{2.5}$ and O_3

3.3.1 Meteorological conditions in January and July

In this study, January and July 2017, when $PM_{2.5}$ and O_3 pollution episodes are likely to occur (Figure 2), are selected to study the role of urbanization. In January 2017, Chengdu experienced $PM_{2.5}$ pollution for 23 out of 31 days with a monthly average concentration of 128.8 μg m^{-3}. From the perspective of atmospheric circulations, westerly winds prevailed over Chengdu due to the large north-south geopotential height gradient at 500 hPa (Figure 4a). However, the westerly winds were blocked by the Tibetan Plateau and thereby the dispersion of $PM_{2.5}$ was limited. At 700 hPa, the southwestern air flow originating from the Bay of Bengal could reach Chengdu (Figure 4b). This warm advection was conducive to the formation of a stable layer near 700 hPa (Figure 4c and d), which made the vertical diffusion of $PM_{2.5}$ difficult. The blocking of air and the stable layer were two important reasons for frequent $PM_{2.5}$ pollution episodes during this period (Hu et al., 2021; Ning et al., 2018).

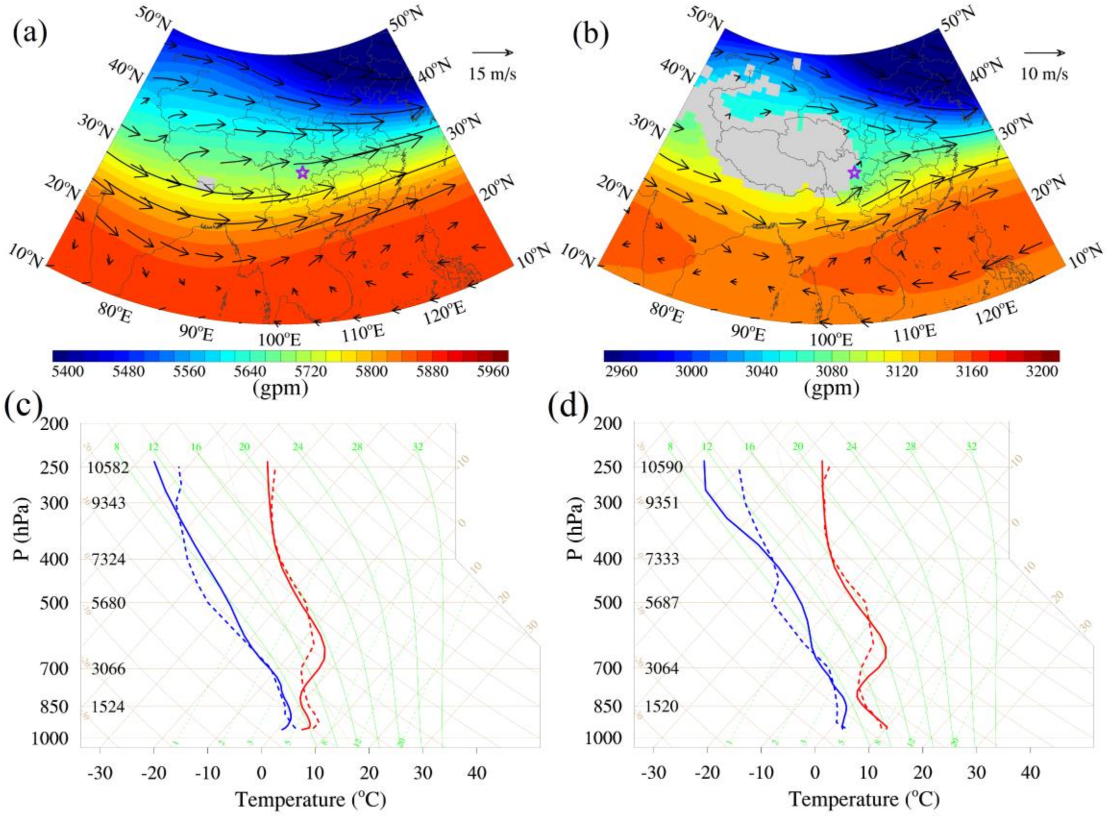

Figure 4. The weather charts at (a) 500 hPa and (b) 700 hPa for January 2017 are based on the NCEP FNL reanalysis data. The purple pentacles show the location of Chengdu. The skew-T diagram at (c) 00:00 UTC and (d) 12:00 UTC in January 2017. The red and blue solid lines are the simulated air temperature and dew point temperature in Jan_Base simulation, while the red and blue dashed lines are the sounding temperature and dew point temperature. These results are monthly averages.

In July 2017, there were 19 days of O_3 pollution in Chengdu, and the monthly average MDA8 O_3 concentration was 172.9 μg m^{-3}. At 500 hPa, Chengdu was dominated by strong high-pressure systems, and thereby air temperature was high and wind speed was small (Figure 5a). The monthly average T_2 was as high as 28.6 ℃ while the monthly average WS_{10} was only 1.6 m s^{-1} during this period (Figure 6b). High temperature favored photochemical reactions of O_3 while weak winds trapped O_3. Furthermore, the thickness of the stable layer in July was far less than that in January (Figure 4c and d; Figure 5c and d). Well-developed boundary layer facilitated vertical mixing of O_3 within the boundary layer, which is an important way to maintain high surface O_3 concentrations during the daytime (Aneja et al., 2000; Tang et al., 2017).

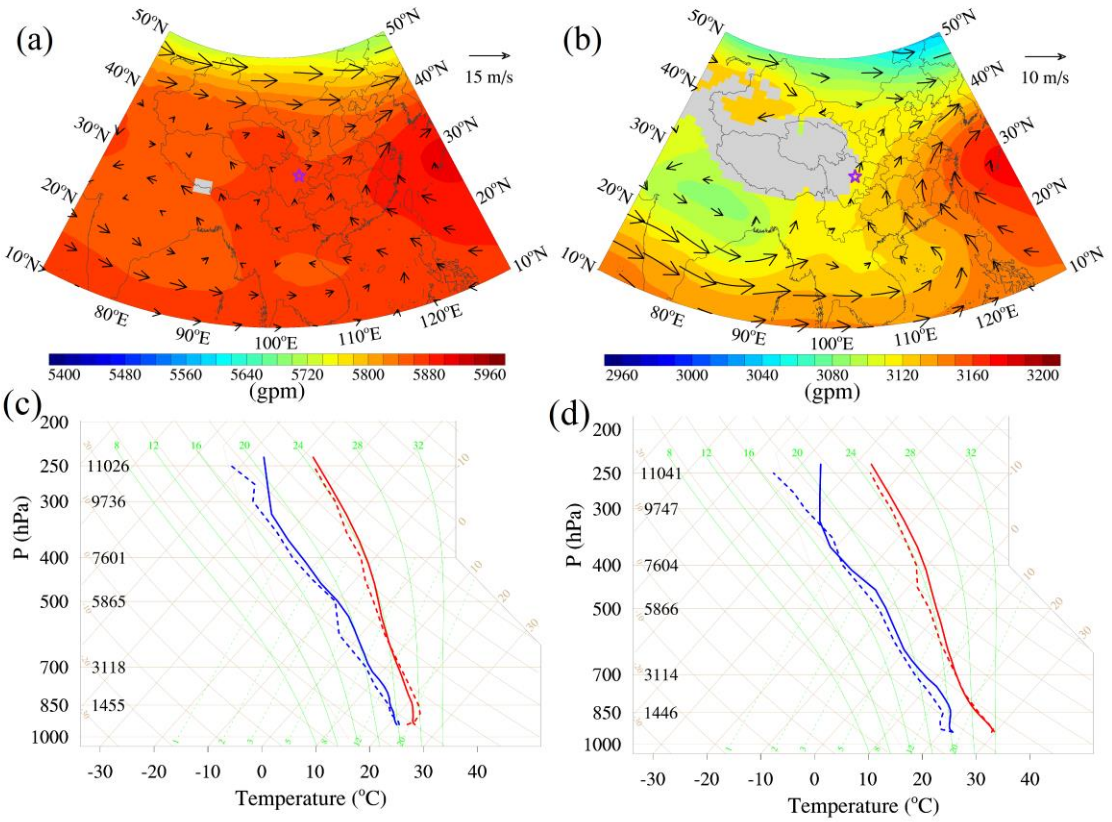

Figure 5. The weather charts at (a) 500 hPa and (b) 700 hPa for July 2017 are based on the NCEP FNL reanalysis data. The purple pentacles show the location of Chengdu. The skew-T diagram at (c) 00:00 UTC and (d) 12:00 UTC in July 2017. The red and blue solid lines are the simulated air temperature and dew point temperature in July_Base simulation, while the red and blue dashed lines are the sounding temperature and dew point temperature. These results are monthly averages.

3.3.2 Evaluation of model performance

We first compare vertical profiles in the model with the sounding data to determine whether the model captures the vertical structure of the troposphere. As shown in Figure 4c-d and 5c-d, the WRF-Chem model can successfully simulate the changes in temperature and dew point temperature in the vertical direction, whether in January or July, day or night. Therefore, the vertical results in the model are reliable. Furthermore, simulated variables are compared observed variables, and the results are presented in Figure 6. The mean bias (MB) of the simulated and observed concentrations of $PM_{2.5}$ and O_3 are 12.7 μg m^{-3} and 11.6 μg m^{-3}, with the normalized mean bias (NMB) values of 9.9% and 12.0%, which are within the acceptable standards (NMB < ± 15%). The correlation coefficients (COR) of $PM_{2.5}$ and O_3 are 0.44 and 0.77, respectively. The statistical metrics for $PM_{2.5}$ and O_3 are similar to those in previous studies (Wang et al., 2022b; Wu et al., 2022), indicating that our model results for $PM_{2.5}$ and O_3 are reasonable and acceptable. With regard to the meteorological variables, T_2 is well simulated with low MB (0.2 and 0.1 °C) and high COR (0.76 and 0.70) values in both January and July. The simulations underestimate TD_2 to some extent with the MB values are –1.5 °C and –2.6 °C in January and July, respectively. As for 10-m wind, poor simulation results are predictable in the case of low wind and complex terrain. The observed calm wind frequency was particularly high due to the starting speed of the anemometer (typically 0.5–1 m s^{-1}), resulting in an overestimation of simulated WS_{10} as in the studies of other scholars (Shu et al., 2021; Wu et al., 2022). This overestimation could also be argued that the unresolved topographic features produce an additional drag to that generated by vegetation, but their effects are not considered in WRF (Jimenez and Dudhia, 2012). The model, on the other hand, captures the shift in wind direction except for the case of calm wind. To sum up, the WRF-Chem model using our configuration has a good capability in simulating $PM_{2.5}$, O_3 and meteorological variables in Chengdu, and thereby the simulations can be used for subsequent analysis.

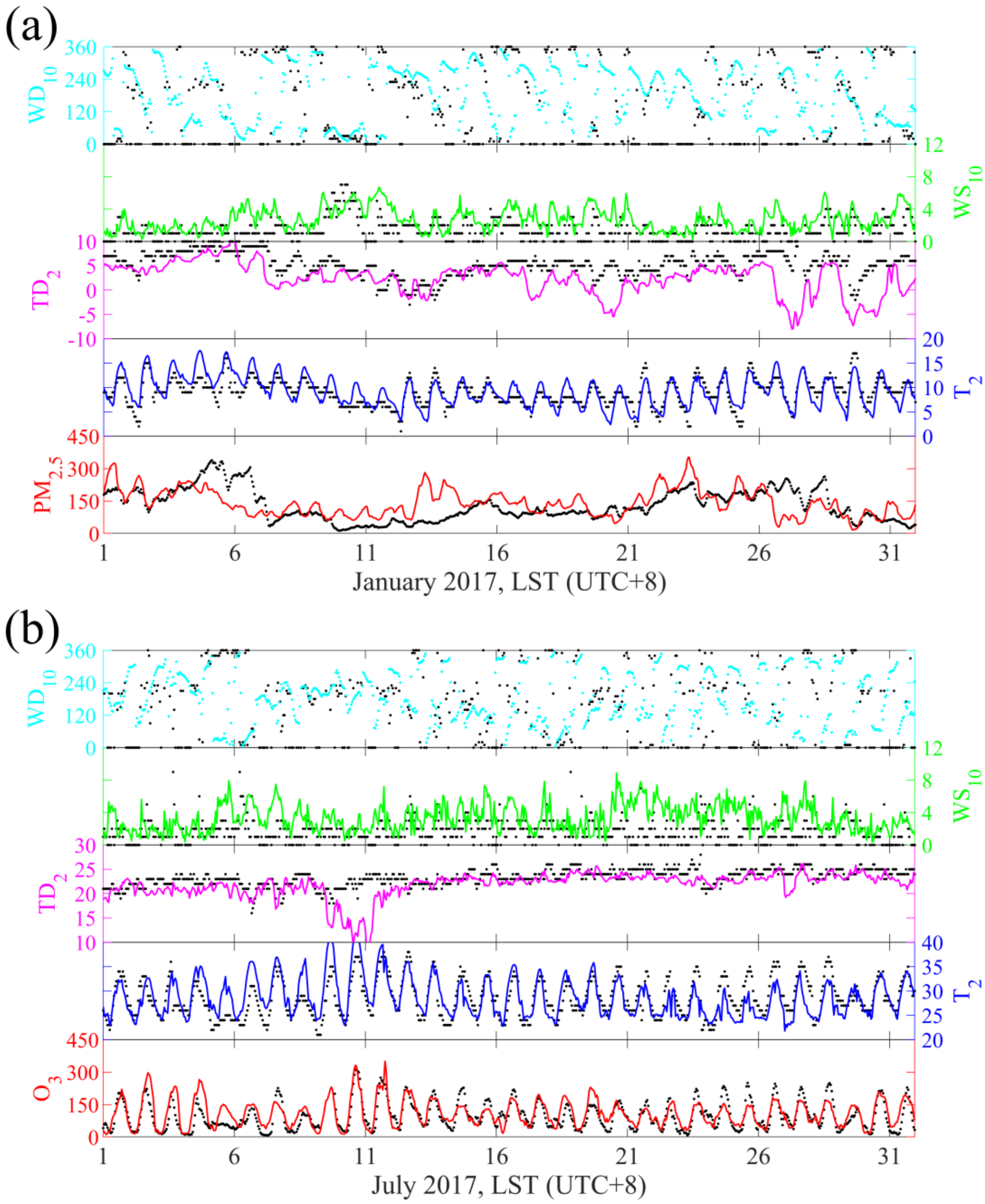

Figure 6. (a) Times series of $PM_{2.5}$, T_2, TD_2, WS_{10} and WD_{10} for January 2017. (b) Times series of O_3, T_2, TD_2 and WS_{10} and WD_{10} for July 2017. The black dots are observations. The colored lines and cyan dots are simulations in baseline simulations.

3.3.3 Spatiotemporal variations in $PM_{2.5}$ and O_3

The spatiotemporal characteristics of $PM_{2.5}$ were first investigated based on the Jan_Base simulation. $PM_{2.5}$ had a diurnal variation with high concentration at night and low concentration at noon, which was contrary to the boundary layer height (Figure 7a). The nocturnal atmospheric boundary layer was often characterized by a stable boundary layer, and the boundary layer height was only ~320 m above ground. As a consequence, $PM_{2.5}$ was trapped and maintained on the ground. The daytime atmospheric boundary layer, also known as the convective boundary layer, could develop to ~1300 m above ground. Turbulence in the convective boundary layer could dilute $PM_{2.5}$ concentrations, resulting in low $PM_{2.5}$ concentrations at surface. Chengdu is on the east side of the Tibetan Plateau, with a large elevation drop exceeding 3000 m over a short horizontal distance (Figure 1a). In this case, the mountain-plain wind can easily form. During nighttime, the mountain wind was characterized by westerly and downslope flow at lower levels along the eastern slope of the Tibetan Plateau (Figure 7b and d). Converging with prevailing northeasterly wind, $PM_{2.5}$ pollution belt was likely to form and could spread hundreds of kilometers downstream. The daytime plain wind was nearly a reversal of the nighttime circulation, with easterly and upslope flow over the Sichuan Basin (Figure 7c and e). The upslope flow could draw $PM_{2.5}$ to a higher elevation, which could also facilitate vertical dispersion of $PM_{2.5}$ during the day.

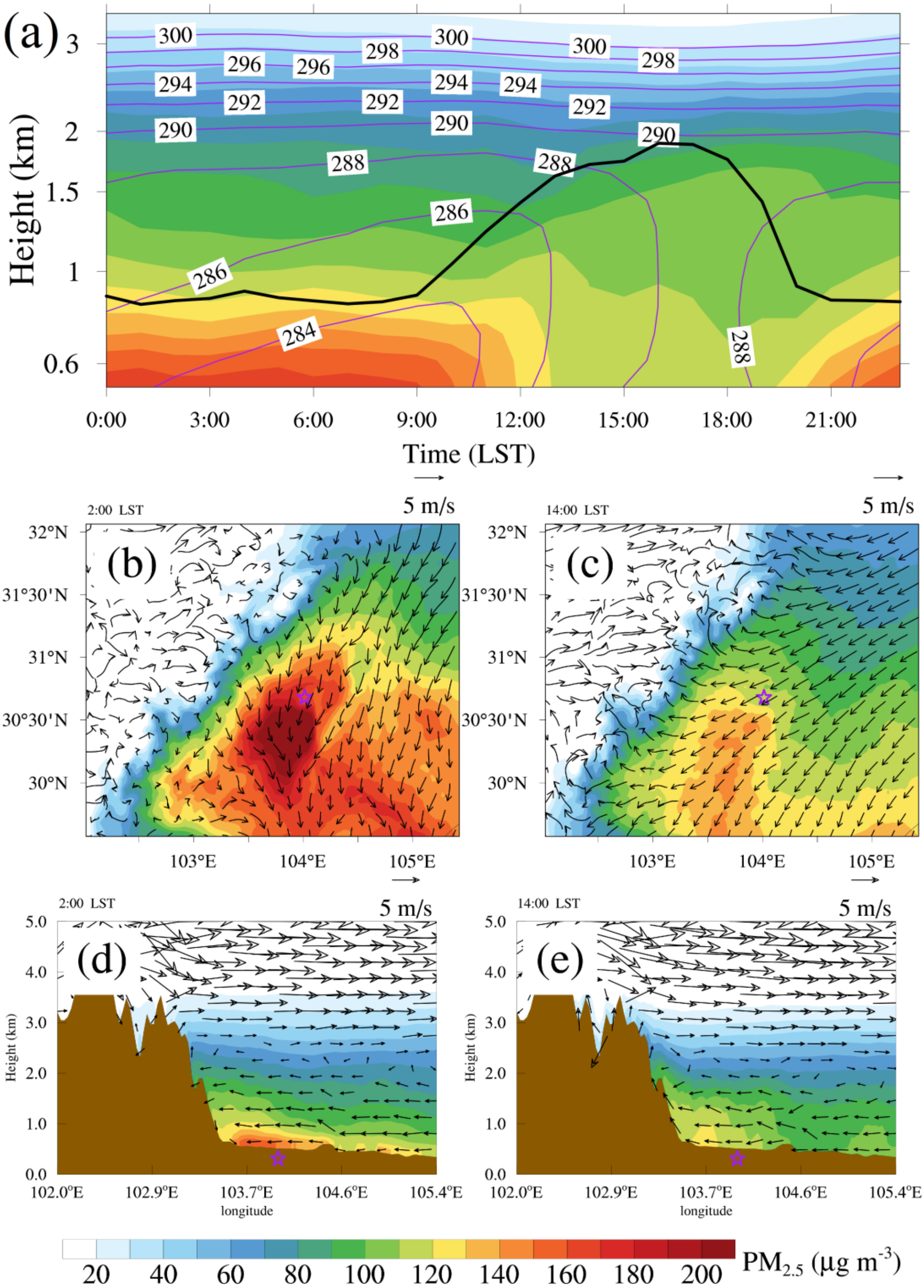

Figure 7. (a) Temporal-vertical cross sections of $PM_{2.5}$ (color shading), potential temperature (purple contour lines) and boundary layer height (thick black contour line) at Chengdu. Horizontal distributions of $PM_{2.5}$ with wind vectors at the lowest model level at (b) 2:00 and (c) 14:00 LST. East-west vertical cross sections of $PM_{2.5}$ with wind vectors at (d) 2:00 and (e) 14:00 LST. Purple pentacles show the locations of Chengdu. Brown-shaded areas represent the terrain. These results are the monthly average based on Jan_Base simulation.

In terms of O_3, it exhibited strong diurnal variation with an afternoon maximum and an early morning minimum (Figure 8a). After sunrise, the nocturnal residual layer was destroyed while the convective boundary layer developed as the surface heated up on account of the incoming radiation. The high-concentration O_3 in the residual layer was then transported downward (Hu et al., 2018). Meanwhile, O_3 could be generated by photochemical reactions between volatile organic compounds (VOCs) and NO_x in the presence of sunlight. Through these two pathways, surface O_3 concentration increased rapidly in the morning (Zhan and Xie, 2022). By noon, O_3 was mixed within the convective boundary layer via strong turbulence. Strong photochemical production and vertical mixing could maintain high surface O_3 concentrations until late afternoon. The daytime plain wind drove the westward transport of O_3 and aggravated O_3 pollution along the eastern slope of the Tibetan Plateau (Figure 8c and e). After sunset, O_3 production ceased as the intensity of sunlight diminished. O_3 concentrations decreased substantially owing to surface deposition and nitrogen oxide titration ($O_3 + NO \rightarrow O_2 + NO_2$), and gradually reached their minimum in the early morning (Figure 8b). But O_3 in the nocturnal residual layer was still at a high level with values of more than 160 $\mu g\ m^{-3}$. The nighttime mountain wind could carry rich-O_3 air eastward and enhanced O_3 concentrations aloft over the eastern slope of the Tibetan Plateau (Figure 8d). Compared with the Jan_Base simulation, O_3 with a concentration of ~100 $\mu g\ m^{-3}$ had always existed over the Tibetan Plateau where $PM_{2.5}$ concentrations were quite low, indicating that the background concentration of O_3 was much higher than that of $PM_{2.5}$. This can pose a huge challenge to O_3 pollution control in Chengdu.

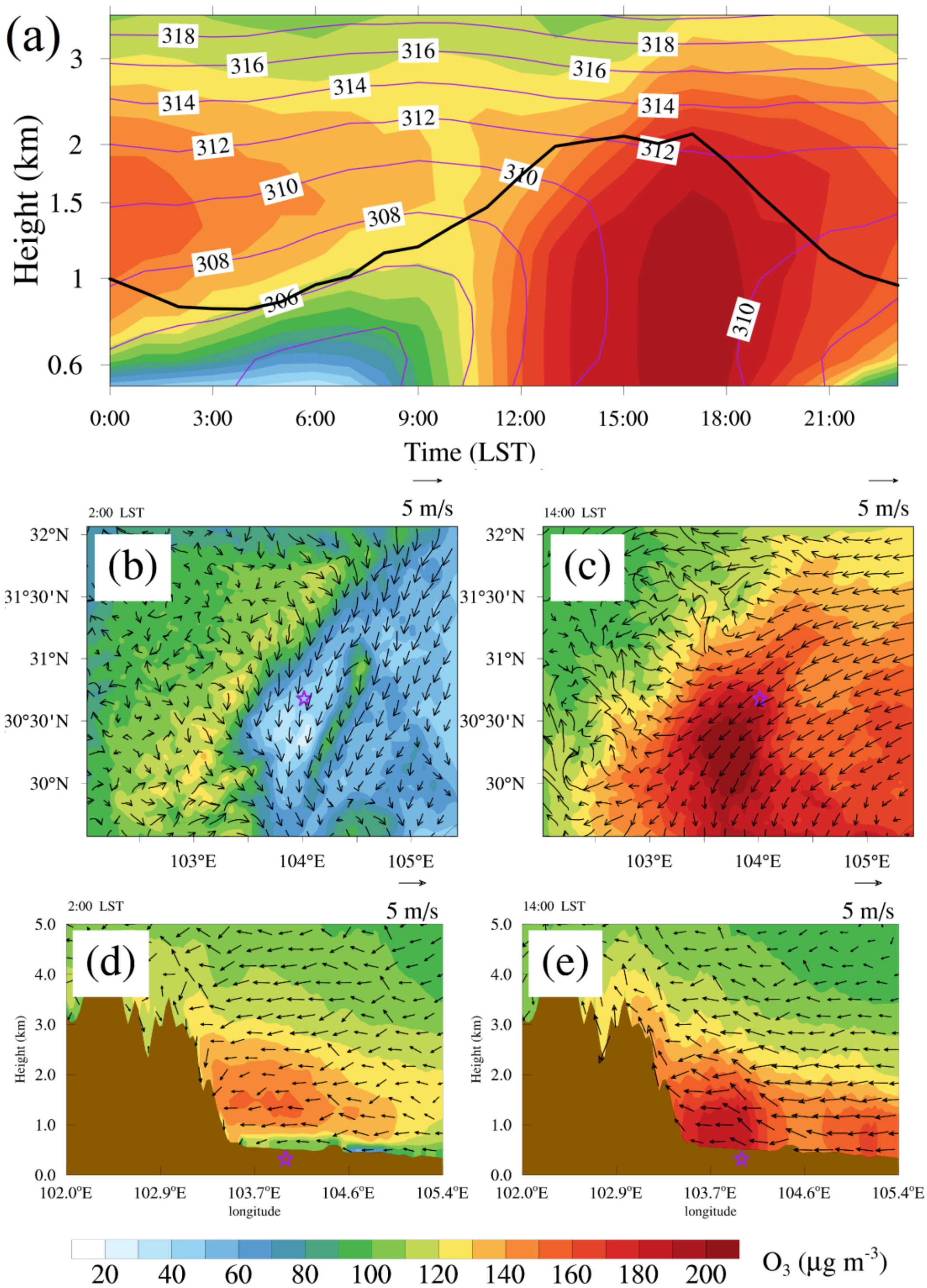

Figure 8. (a) Temporal-vertical cross sections of O_3 (color shading), potential temperature (purple contour lines) and boundary layer height (thick black contour lines) at Chengdu. Horizontal distributions of O_3 with wind vectors at the lowest model level at (b) 2:00 and (c) 14:00 LST. East-west vertical cross sections of O_3 with wind vectors at (d) 2:00 and (e) 14:00 LST. Purple pentacles show the locations of Chengdu. Brown-shaded areas represent the terrain. These results are the monthly average based on July_Base simulation.

3.3.4 Impacts of urban land use on $PM_{2.5}$ and O_3

Modification of urban land use changes surface dynamic and thermal characteristics, affecting the exchange of energy, moisture and momentum and hence altering urban meteorology and air quality. As illustrated in Figure 9, surface $PM_{2.5}$ concentrations in Jan_Base simulation were lower than those in Jan_noCD simulation, with the monthly average concentrations decreased by 10.8 μg m^{-3} (7.6%). Moreover, the decrease in $PM_{2.5}$ concentrations was larger during nighttime than during daytime. The monthly average $PM_{2.5}$ concentrations decreased by 13.9 μg m^{-3} (8.6%) at 2:00 LST (LST is UTC+8h) but only 3.0 μg m^{-3} (2.6%) at 14:00 LST (Figure 9a and b). The decrease in surface $PM_{2.5}$ concentrations was mainly attributed to the modification of the boundary layer height. Urban land use can enhance surface heating and then increases air temperature. The vertical air movement is then enhanced by the warming up of air temperature, increasing the boundary layer height (Figure S1), which facilitates the vertical diffusion of surface $PM_{2.5}$. $PM_{2.5}$ concentrations increased by 2–6 μg m^{-3} in the upper boundary layer (~1 km above ground) (Figure 9c and d), further confirming this point.

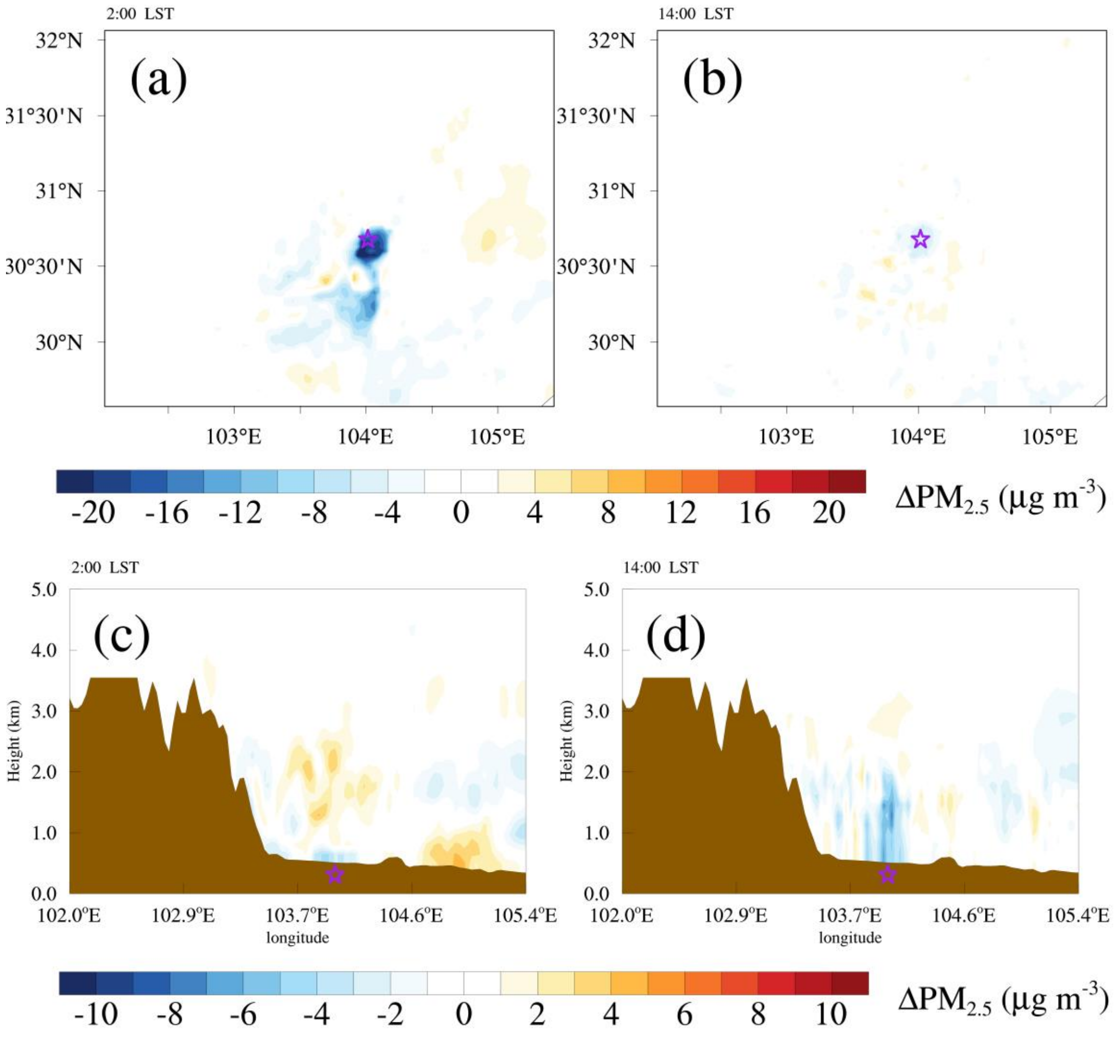

Figure 9. Horizontal distributions of the differences in $PM_{2.5}$ at the lowest model level at (a) 2:00 and (b) 14:00 LST. East-west vertical cross sections of the difference in $PM_{2.5}$ at (c) 2:00 and (d) 14:00 LST. Purple pentacles show the location of Chengdu. Brown-shaded areas represent the terrain. These results are the difference between the monthly average of Jan_Base and Jan_noCD simulations (Jan_Base minus Jan_noCD).

O_3 is a secondary air pollutant that is not only related to meteorological conditions but also its precursors (VOCs and NO_x). Due to the increase in upward air movement and boundary layer height induced by urban land use compared to cropland (Figure S2), like $PM_{2.5}$, NO_x concentrations also decreased near the surface (Liao et al., 2015; Zhu et al., 2017). The decrease in NO_x near the surface resulted in an increase in surface O_3 at night since the NO_x titration was weakened (Figure 10a and c). Although the elevated boundary layer diluted O_3 concentrations to some extent, the nighttime O_3

concentrations were mainly dominated by chemical effects and increased by 15.6 μg m^{-3} (16.0%) at 2:00 LST (Figure 10a). During daytime, the increased air temperature was conducive to the photochemical production of O_3, and the well-developed convective boundary layer favored the vertical mixing of O_3. O_3 concentrations would also increase (Figure 10b and d), with the monthly average value increasing by 5.4 μg m^{-3} (4.5%) at 14:00 LST. Since high O_3 concentrations were mainly concentrated in the afternoon, the monthly average MDA8 O_3 concentrations finally increased by 10.6 μg m^{-3} (6.0%) due to the effects of urban expansion.

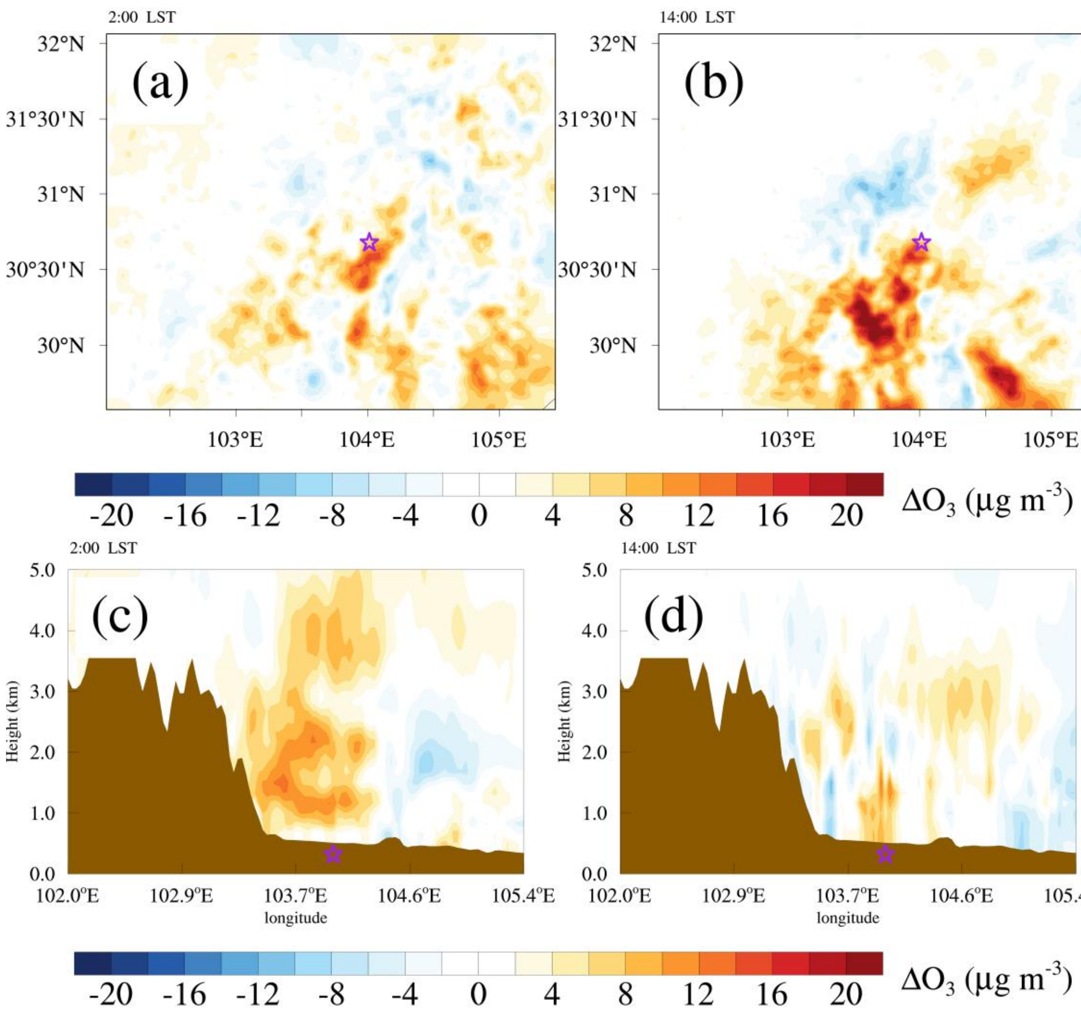

Figure 10. Horizontal distributions of the differences in O_3 at the lowest model level at (a) 2:00 and (b) 14:00 LST. East-west vertical cross sections of the difference in O_3 at (c) 2:00 and (d) 14:00 LST. Purple pentacles show the location of Chengdu. Brown-shaded areas represent the terrain. These results are the difference between the monthly average of July_Base and July_noCD simulations (July_Base minus July_noCD).

3.3.5 Impacts of anthropogenic emissions on $PM_{2.5}$ and O_3

Rising anthropogenic emissions of air pollutants and their precursors can significantly increase ambient air pollution. Therefore, the impacts of anthropogenic emissions are more intuitive than urban land use. Figure 11 shows the differences in $PM_{2.5}$ between the monthly average of Jan_Base and Jan_noEmi simulations (Jan_Base minus Jan_noEmi). $PM_{2.5}$ concentrations in Jan_Base simulation were significantly higher than those in Jan_noEmi simulation, with the monthly average concentration increased by 23.9 μg m^{-3} (16.8%), more than twice the difference between Jan_Base and Jan_noCD simulations. Furthermore, the increases in $PM_{2.5}$ concentrations appeared throughout the boundary layer (Figure 11c and d) and could extend downstream for hundreds of kilometers (Figure 11a and b), indicating that reducing anthropogenic emissions is an effective way to reduce $PM_{2.5}$ concentrations.

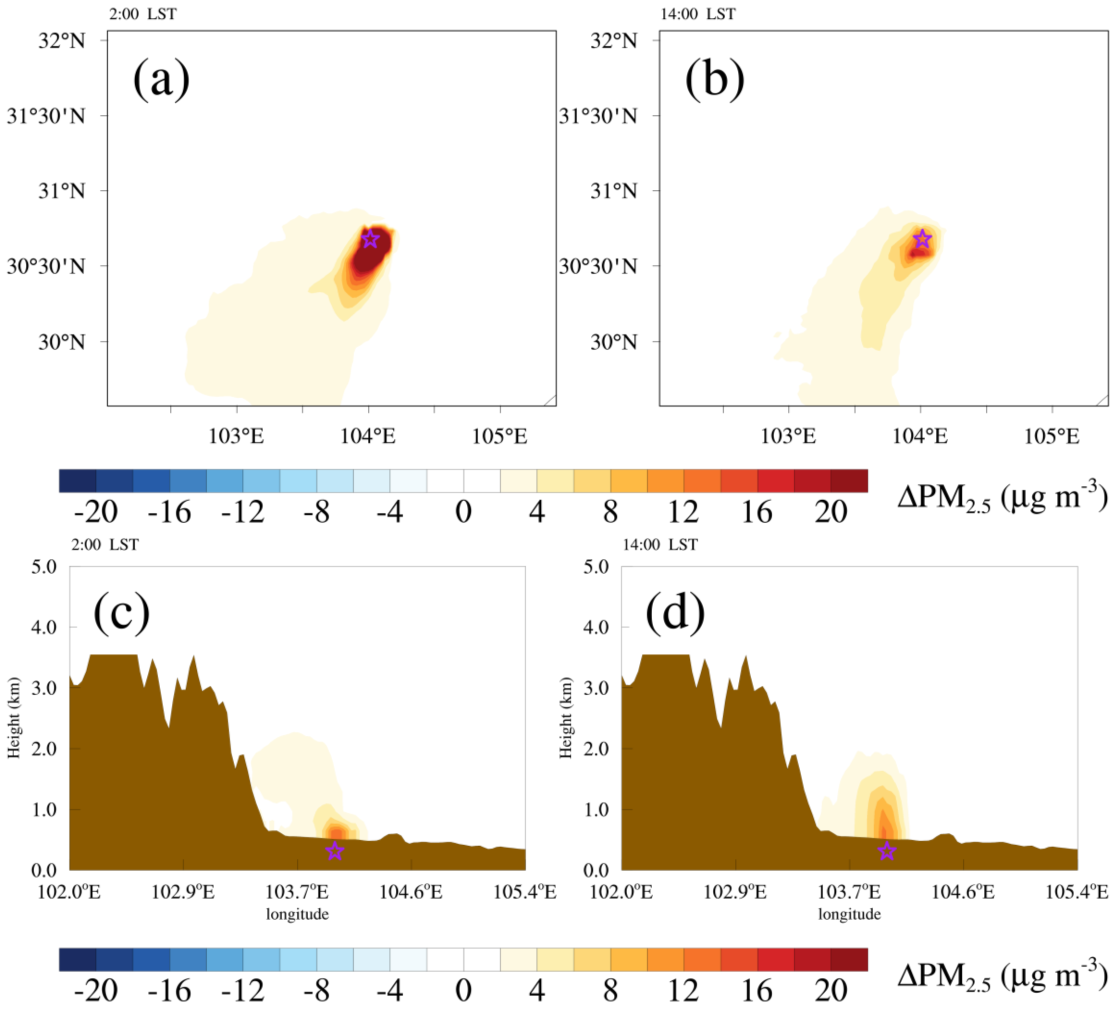

Figure 11. Same as Figure 9, but for the difference between the monthly average of Jan_Base

and Jan_noEmi simulations (Jan_Base minus Jan_noEmi).

As for O_3, the monthly average O_3 concentrations in July_Base simulation were only 1.6 μg m^{-3} (1.4%) higher than those in July_noEmis simulation at 14:00 LST (Figure 12b and d), which was much smaller than the change in $PM_{2.5}$. This phenomenon may be related to the non-linear sensitivity of O_3 to VOCs and NO_x precursor emissions. O_3 formation regimes can be classified into VOC-limited, NO_x-limited and transition regimes depending on the ratio of VOCs and NO_x (Jin et al., 2020; Lu et al., 2019). At low VOC/NO_x ratios (VOC-limited regime), reducing the concentrations of NO_x would even lead to an increase in O_3 formation. Considering Chengdu remained VOC-limited regime during 2013 to 2020 (Tian et al., 2018; Wang et al., 2022), the effects of reducing NO_x emissions may be partially offset by changes in VOCs, and thereby a reasonable regulation framework that involves joint control of NO_x and VOC emissions is necessary to alleviate O_3 pollution. Although the presence of anthropogenic emissions reduced the monthly average O_3 concentrations by 3.0 μg m^{-3} (3.1%) at 2:00 LST, the monthly average MDA8 O_3 concentrations in July_Base simulation were 4.8 μg m^{-3} (2.7%) higher than those in July_noEmis simulation.

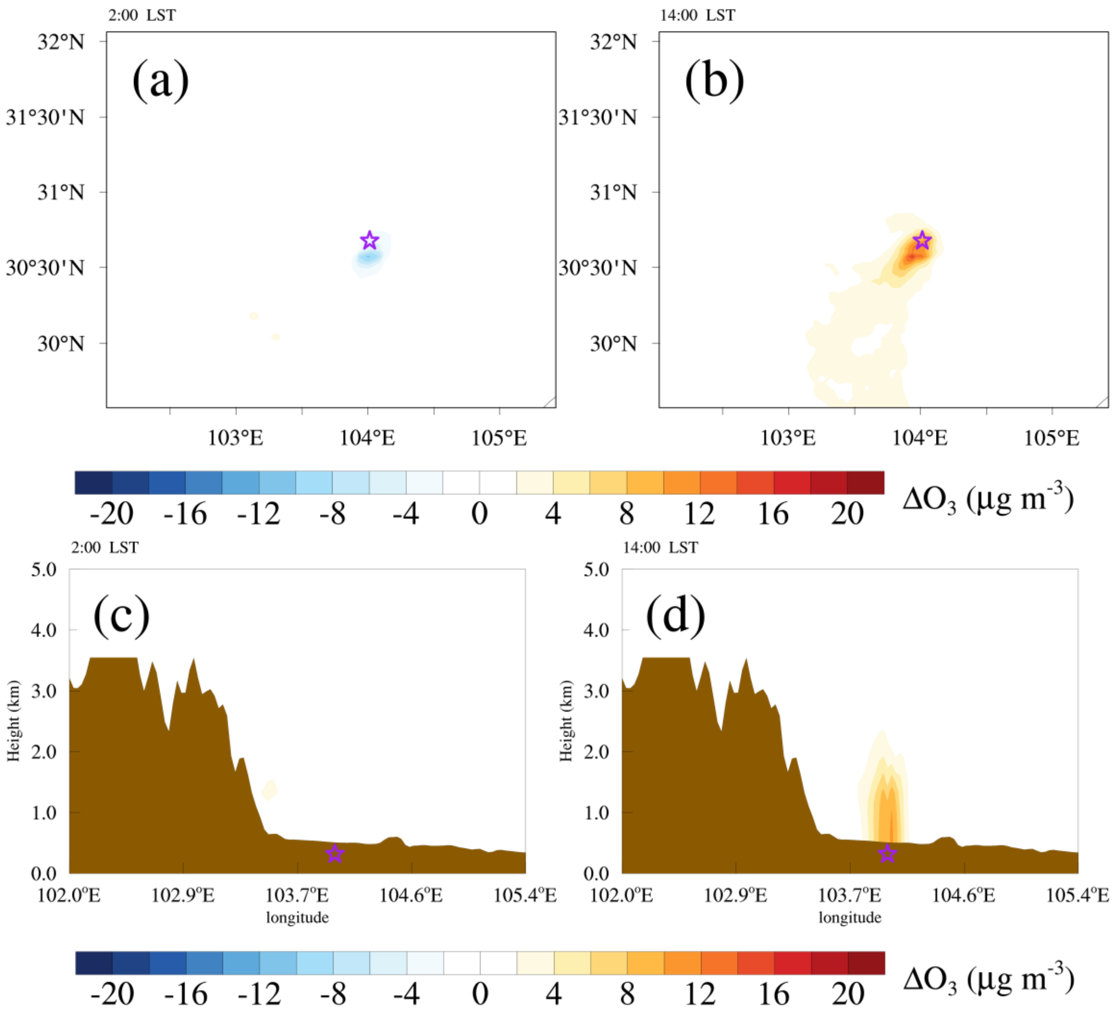

Figure 12. Same as Figure 10, but for the difference between the monthly average of July_Base and July_noEmi simulations (July_Base minus July_noEmi).

3.4 Health risks caused by urbanization

According to the above results, urban land use decreased the monthly average of $PM_{2.5}$ concentrations by 10.8 μg m^{-3} (7.6%) but increased the monthly average of MDA8 O_3 concentrations by 10.6 μg m^{-3} (6.0%). On the other hand, anthropogenic emissions increased both $PM_{2.5}$ and MDA8 O_3 concentrations, with monthly average values of 23.9 μg m^{-3} (16.8%) and 4.8 μg m^{-3} (2.7%), respectively. We then calculate the changes in premature mortalities under different simulation scenarios to assess the health risks from changes in $PM_{2.5}$ and O_3 concentrations. As shown in Figure 13, the premature mortalities from ANAC, CVD, RD and COPD due to $PM_{2.5}$ decreased by 171 (95%CI: 129–200, or about 6.9%), 45 (95%CI: 34–53, or about 6.7%), 22 (95%CI: 16–27, or about 6.5%) and 23 (95%CI: 17–26, or about 6.2%) in January 2017 when Chengdu area was urban land use rather than cropland. On the other hand, anthropogenic emissions in Chengdu increased premature mortalities from ANAC, CVD, RD and COPD due to $PM_{2.5}$ by 388 (95%CI: 291–456, or about 15.7%), 102 (95%CI: 77–121, or about 15.1%), 51 (95%CI: 35–62, or about 15.0%) and 52 (95%CI: 39–60, or about 14.1%). With regard to O_3, premature mortalities from O_3-induced diseases all increased when urban land use and anthropogenic emissions were taken into account. Urban land use led to an increase in premature mortalities from ANAC, CVD, RD and COPD due to O_3 by 203 (95%CI: 122–268, or about 9.5%), 51 (95%CI: 22–71, or about 9.4%), 18 (95%CI: –14–35, or about 10.0%) and 17 (95%CI: –15–33, or about 9.7%) in July 2017 compared to cropland. When anthropogenic emissions in Chengdu were turned on, premature mortalities from ANAC, CVD, RD and COPD due to O_3 increased by 87 (95%CI: 54–112, or about 4.1%), 22 (95%CI: 10–29, or about 4.1%), 8 (95%CI: –7–14, or about 4.4%) and 7 (95%CI: –7–13, or about 4.0%), respectively. In summary, the total premature mortalities due to $PM_{2.5}$ and O_3 changed by about –6.9% and 9.5% affected by urban expansion, and these values changed to about 15.7% and 4.1% affected by emissions growth.

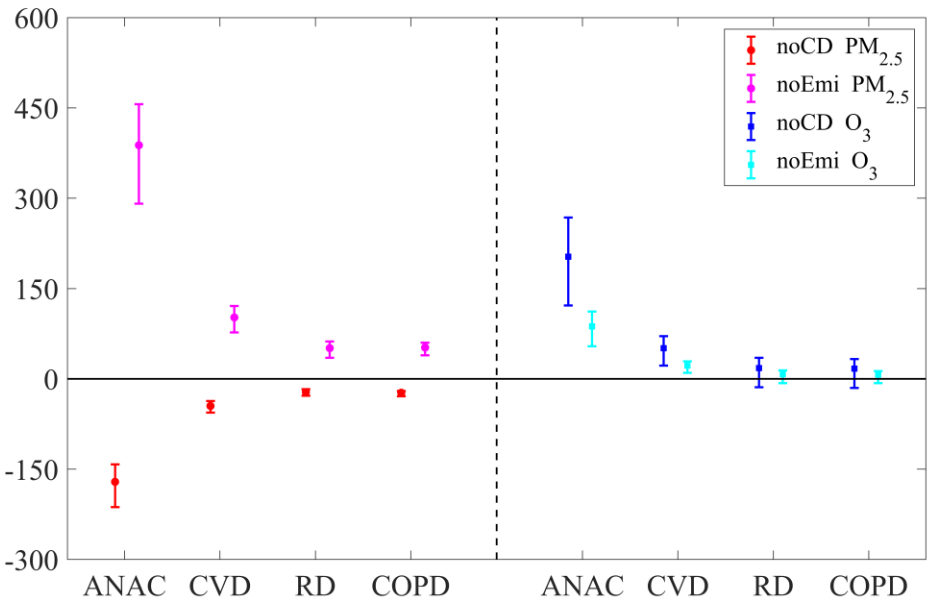

Figure 13. Differences in premature mortality from ANAC, CVD, RD and COPD due to $PM_{2.5}$ (left of the dotted line) and O_3 (right of the dotted line) between baseline and sensitivity simulations. The dots represent the mean estimate, and the whiskers represent 95% confidence intervals.

4 Conclusions

With the development in urbanization, urban land use and anthropogenic emissions increase, which affects urban air quality and then health risks of air pollutants. In this study, the impacts of urban land use and anthropogenic emissions on air pollutant concentrations and the related health risks in Chengdu, a highly urbanized city with severe air pollution and complex terrain, are quantified. Management of urban air pollution is usually achieved by reducing anthropogenic emissions. Thus, the effects of urban expansion are further compared with those of emissions growth.

Chengdu is suffering from severe $PM_{2.5}$ and O_3 pollution in recent years. There were 97, 101, 68, 53, 33, 43 and 37 $PM_{2.5}$ pollution episodes, and 61, 48, 42, 40, 42, 71 and 48 O_3 pollution episodes from 2015 to 2021. Severe $PM_{2.5}$ and O_3 pollution posed huge health risks. The 7-year annual averages of premature mortalities from ANAC, CVD, RD and COPD due to $PM_{2.5}$ were 9386 (95%CI: 6542–11726), 2609 (95%CI: 1788–3384), 1321(95%CI: 804–1840) and 1485 (95%CI: 941–1983), those due to O_3 were 8506 (95%CI: 4817–11882), 2175 (95%CI: 863–3320), 713 (95%CI: –492–1664) and 693 (95%CI: –517–1617). $PM_{2.5}$ and O_3 pollution had different seasonal preferences. Owing to the blocking of air and the stable atmospheric layer, $PM_{2.5}$ pollution tended to appear in cold months (November to February). However, O_3 pollution was likely to occur in warm months (April to August) because of the high temperature and strong sunlight dominated by high-pressure systems. $PM_{2.5}$ concentrations were high at night and low at noon, which was contrary to the boundary layer height. O_3 exhibited strong diurnal variation with an afternoon maximum and an early morning minimum, which was related to photochemical reactions during daytime and nitrogen oxide titration at night.

The urban land use of Chengdu was replaced by cropland in the WRF-Chem model to examine the impacts of urban expansion. Urban land use led to an increase in air temperature and boundary layer height compared to cropland, and decreased monthly averaged surface $PM_{2.5}$ concentrations by 10.8 μg m^{-3} (7.6%). Higher temperature and boundary layer height increased O_3 concentrations via stronger photochemical reactions and better vertical mixing during daytime. During nighttime, dominated by the weakened chemical NO_x titration, O_3 concentrations also increased. The monthly averaged MDA8 O_3 concentrations finally increased by 10.6 μg m^{-3} (6.0%). In this case, when Chengdu area was urban land use rather than cropland, the premature mortalities from ANAC due to $PM_{2.5}$ exposure decreased by 171 (95%CI: 129–200, or about 6.9%) but those due to O_3 increased by 203 (95%CI: 122–268, or about 9.5%). Anthropogenic emissions increased surface $PM_{2.5}$ significantly with the monthly average concentration increasing by 23.9 μg m^{-3} (16.8%), more than twice the difference caused by urban land use. Owing to the non-linear sensitivity of O_3 to its precursors, O_3 concentrations increased at noon but decreased at night. In particular, the monthly average O_3 concentrations increased by 1.6 μg m^{-3} (1.4%) at 14:00 LST but decreased by 3.0 μg m^{-3} (3.1%) at 2:00 LST. Since O_3 concentrations in daytime were much higher than those at night, the monthly average MDA8 O_3 concentrations still increased by 4.8 μg m^{-3} (2.7%). As a consequence, the premature mortalities from ANAC due to $PM_{2.5}$ increased by 388 (95%CI: 291–456, or about 15.7%), and those due to O_3 increased by 87 (95%CI: 54–112, or about 4.1%) with anthropogenic emissions in Chengdu.

Our results show that the impacts of urban expansion (about –6.9% for $PM_{2.5}$ and about 9.5% for O_3) are in the same order as those induced by emissions growth (about 15.7% for $PM_{2.5}$ and about 4.1% for O_3) on air pollutants. This suggests that although the focus of air quality management is traditionally to regulate emissions, urban planning is an ancillary option and should also be considered in future air pollution strategies.

Data Availability Statement.

Air quality monitoring data are acquired from the official NEMC real-time publishing platform (http://106.37.208.233:20035/). Meteorological data are taken from the website of the University of Wyoming (http://weather.uwyo.edu/). The NCEP FNL data were taken from the NCEP (https://doi.org/10.5065/D6M043C6/). The MEIC data are accessible at http://meicmodel.org/. These data can be downloaded for free as long as you agree to the official instructions.

Author contributions.

CZ and MX had the original ideas, designed the research, collected the data and prepared the original draft. CZ did the numerical simulations and carried out the data analysis. MX acquired financial support for the project leading to this publication. HL, BL and ZW collected the data. TW, BZ, ML and SL reviewed the initial draft and checked the language of the original draft.

Competing interests.

The contact author has declared that neither they nor their co-authors have any competing interests.

Acknowledgements.

We are grateful to NEMC for the air quality monitoring data, to NCDC for the meteorological data, to NCEP for global final analysis fields and to Tsinghua University for the MEIC inventories. The numerical calculations were performed on the Blade cluster system in the High Performance Computing and Massive Data Center (HPC&MDC) of School of Atmospheric Sciences, Nanjing University. We thank the anonymous reviewers for their constructive comments and suggestions.

Financial support.

This work was supported by the National Nature Science Foundation of China (grant no. 42275102), the open research fund of Chongqing Meteorological Bureau (KFJJ-201607) and the Natural Science Foundation of Jiangsu Province (grant no. BK20211158).

References

Aneja, V. P., Mathur, R., Arya, S. P., Li, Y. X., Murray, G. C., and Manuszak, T. L.: Coupling the vertical distribution of ozone in the atmospheric boundary layer, Environ. Sci. Technol., 34, 2324-2329, https://doi.org/10.1021/es990997+, 2000.

Anenberg, S. C., Horowitz, L. W., Tong, D. Q., and West, J. J.: An estimate of the global burden of anthropogenic ozone and fine particulate matter on premature human mortality using atmospheric modeling, Environ Health Perspect, 118, 1189-1195, https://doi.org/10.1289/ehp.0901220, 2010.

Baasandorj, M., Hoch, S. W., Bares, R., Lin, J. C., Brown, S. S., Millet, D. B., Martin, R., Kelly, K., Zarzana, K. J., Whiteman, C. D., Dube, W. P., Tonnesen, G., Jaramillo, I. C., and Sohl, J.: Coupling between Chemical and Meteorological Processes under Persistent Cold-Air Pool Conditions: Evolution of Wintertime $PM_{2.5}$ Pollution Events and N_2O_5 Observations in Utah's Salt Lake Valley, Environ Sci Technol, 51, 5941-5950, https://doi.org/10.1021/acs.est.6b06603, 2017.

Bahreini, R., Ahmadov, R., McKeen, S. A., Vu, K. T., Dingle, J. H., Apel, E. C., Blake, D. R., Blake, N., Campos, T. L., Cantrell, C., Flocke, F., Fried, A., Gilman, J. B., Hills, A. J., Hornbrook, R.

S., Huey, G., Kaser, L., Lerner, B. M., Mauldin, R. L., Meinardi, S., Montzka, D. D., Richter, D., Schroeder, J. R., Stell, M., Tanner, D., Walega, J., Weibring, P., and Weinheimer, A.: Sources and characteristics of summertime organic aerosol in the Colorado Front Range: perspective from measurements and WRF-Chem modeling, Atmos. Chem. Phys., 18, 8293-8312, https://doi.org/10.5194/acp-18-8293-2018, 2018.

Baklanov, A., Molina, L. T., and Gauss, M.: Megacities, air quality and climate, Atmospheric Environment, 126, 235-249, https://doi.org/10.1016/j.atmosenv.2015.11.059, 2016.

Brauer, M., Freedman, G., Frostad, J., van Donkelaar, A., Martin, R. V., Dentener, F., van Dingenen, R., Estep, K., Amini, H., Apte, J. S., Balakrishnan, K., Barregard, L., Broday, D., Feigin, V., Ghosh, S., Hopke, P. K., Knibbs, L. D., Kokubo, Y., Liu, Y., Ma, S. F., Morawska, L., Sangrador, J. L. T., Shaddick, G., Anderson, H. R., Vos, T., Forouzanfar, M. H., Burnett, R. T., and Cohen, A.: Ambient Air Pollution Exposure Estimation for the Global Burden of Disease 2013, Environ. Sci. Technol., 50, 79-88, https://doi.org/10.1021/acs.est.5b03709, 2016.

Chen, S. H. and Sun, W. Y.: A one-dimensional time dependent cloud model, J. Meteorol. Soc. Jpn., 80, 99-118, https://doi.org/10.2151/jmsj.80.99, 2002.

Chen, R., Yin, P., Meng, X., Liu, C., Wang, L., Xu, X., Ross, J. A., Tse, L. A., Zhao, Z., Kan, H., and Zhou, M.: Fine Particulate Air Pollution and Daily Mortality. A Nationwide Analysis in 272 Chinese Cities, Am J Respir Crit Care Med, 196, 73-81, https://doi.org/10.1164/rccm.201609-1862OC, 2017.

Dai, X. A., Johnson, B. A., Luo, P. L., Yang, K., Dong, L. X., Wang, Q., Liu, C., Li, N. W., Lu, H., Ma, L., Yang, Z. L., and Yao, Y. Z.: Estimation of Urban Ecosystem Services Value: A Case Study of Chengdu, Southwestern China, Remote Sens., 13, 24, https://doi.org/10.3390/rs13020207, 2021.

Fast, J. D., Gustafson, W. I., Easter, R. C., Zaveri, R. A., Barnard, J. C., Chapman, E. G., Grell, G. A., and Peckham, S. E.: Evolution of ozone, particulates, and aerosol direct radiative forcing in the vicinity of Houston using a fully coupled meteorology-chemistry-aerosol model, J. Geophys. Res.-Atmos., 111, 29, https://doi.org/10.1029/2005jd006721, 2006.

Grell, G. A. and Devenyi, D.: A generalized approach to parameterizing convection combining ensemble and data assimilation techniques, Geophys. Res. Lett., 29, 4, https://doi.org/10.1029/2002gl015311, 2002.

Grell, G. A., Peckham, S. E., Schmitz, R., McKeen, S. A., Frost, G., Skamarock, W. C., and Eder, B.: Fully coupled “online” chemistry within the WRF model, Atmospheric Environment, 39, 6957-6975, https://doi.org/10.1016/j.atmosenv.2005.04.027, 2005.

Guenther, A., Karl, T., Harley, P., Wiedinmyer, C., Palmer, P. I., and Geron, C.: Estimates of global terrestrial isoprene emissions using MEGAN (Model of Emissions of Gases and Aerosols from Nature), Atmos. Chem. Phys., 6, 3181-3210, https://doi.org/10.5194/acp-6-3181-2006, 2006.

Guo, H., Ling, Z. H., Cheung, K., Jiang, F., Wang, D. W., Simpson, I. J., Barletta, B., Meinardi, S., Wang, T. J., Wang, X. M., Saunders, S. M., and Blake, D. R.: Characterization of photochemical pollution at different elevations in mountainous areas in Hong Kong, Atmos. Chem. Phys., 13, 3881-3898, https://doi.org/10.5194/acp-13-3881-2013, 2013.

Holman, C., Harrison, R. M., and Querol, X.: Review of the efficacy of low emission zones to improve urban air quality in European cities, Atmospheric Environment, 111, 161-169, https://doi.org/10.1016/j.atmosenv.2015.04.009, 2015.

Hu, Y. and Wang, S.: Formation mechanism of a severe air pollution event: A case study in the Sichuan Basin, Southwest China, Atmospheric Environment, 246, https://doi.org/10.1016/j.atmosenv.2020.118135, 2021.

Hu, J., Li, Y. C., Zhao, T. L., Liu, J., Hu, X. M., Liu, D. Y., Jiang, Y. C., Xu, J. M., and Chang, L. Y.: An important mechanism of regional O-3 transport for summer smog over the Yangtze River Delta in eastern China, Atmos. Chem. Phys., 18, 16239-16251, https://doi.org/10.5194/acp-18-16239-2018, 2018.

Janjic, Z. I.: THE STEP-MOUNTAIN ETA COORDINATE MODEL - FURTHER DEVELOPMENTS OF THE CONVECTION, VISCOUS SUBLAYER, AND TURBULENCE CLOSURE SCHEMES, Mon. Weather Rev., 122, 927-945, https://doi.org/10.1175/1520-0493(1994)122<0927:Tsmecm>2.0.Co;2, 1994.

Jimenez, P. A. and Dudhia, J.: Improving the Representation of Resolved and Unresolved Topographic Effects on Surface Wind in the WRF Model, J. Appl. Meteorol. Climatol., 51, 300-316, https://doi.org/10.1175/jamc-d-11-084.1, 2012.

Jin, X. M., Fiore, A., Boersma, K. F., De Smedt, I., and Valin, L.: Inferring Changes in Summertime Surface Ozone-NOx-VOC Chemistry over US Urban Areas from Two Decades of Satellite and Ground-Based Observations, Environ. Sci. Technol., 54, 6518-6529, https://doi.org/10.1021/acs.est.9b07785, 2020.

Karl, T., Gohm, A., Rotach, M. W., Ward, H. C., Graus, M., Cede, A., Wohlfahrt, G., Hammerle, A., Haid, M., Tiefengraber, M., Lamprecht, C., Vergeiner, J., Kreuter, A., Wagner, J., and Staudinger, M.: Studying Urban Climate and Air Quality in the Alps: The Innsbruck Atmospheric Observatory, Bull. Amer. Meteorol. Soc., 101, E488-E507, https://doi.org/10.1175/bams-d-19-0270.1, 2019.

Kinney, P. L.: Interactions of Climate Change, Air Pollution, and Human Health, Curr. Environ. Health Rep., 5, 179-186, https://doi.org/10.1007/s40572-018-0188-x, 2018.

Lee, C. S. L., Chou, C. C., Cheung, H. C., Tsai, C. Y., Huang, W. R., Huang, S. H., Chen, M. J., Liao, H. T., Wu, C. F., Tsao, T. M., Tsai, M. J., and Su, T. C.: Seasonal variation of chemical characteristics of fine particulate matter at a high-elevation subtropical forest in East Asia, Environ Pollut, 246, 668-677, https://doi.org/10.1016/j.envpol.2018.11.033, 2019.

Lelieveld, J., Barlas, C., Giannadaki, D., and Pozzer, A.: Model calculated global, regional and megacity premature mortality due to air pollution, Atmos. Chem. Phys., 13, 7023-7037, https://doi.org/10.5194/acp-13-7023-2013, 2013.

Liao, J., Wang, T., Jiang, Z., Zhuang, B., Xie, M., Yin, C., Wang, X., Zhu, J., Fu, Y., and Zhang, Y.: WRF/Chem modeling of the impacts of urban expansion on regional climate and air pollutants in Yangtze River Delta, China, Atmospheric Environment, 106, 204-214, https://doi.org/10.1016/j.atmosenv.2015.01.059, 2015.

Lin, B. and Zhu, J.: Changes in urban air quality during urbanization in China, J. Clean Prod., 188, 312-321, https://doi.org/10.1016/j.jclepro.2018.03.293, 2018.

Liu, H., Liu, S., Xue, B., Lv, Z., Meng, Z., Yang, X., Xue, T., Yu, Q., and He, K.: Ground-level ozone pollution and its health impacts in China, Atmospheric Environment, 173, 223-230, https://doi.org/10.1016/j.atmosenv.2017.11.014, 2018.

Lu, H. X., Lyu, X. P., Cheng, H. R., Ling, Z. H., and Guo, H.: Overview on the spatial-temporal characteristics of the ozone formation regime in China, Environ. Sci.-Process Impacts, 21, 916-929, https://doi.org/10.1039/c9em00098d, 2019.

Luo, Y. L., Shen, J., Chen, A. F., Tao, Q., Li, Q. Q., White, P. J., Li, T. Q., Li, B., Chen, L., Li, H. X., Gao, X. S., Xu, Q., and Wang, C. Q.: Loss of organic carbon in suburban soil upon urbanization of Chengdu megacity, China, Sci. Total Environ., 785, 10, https://doi.org/10.1016/j.scitotenv.2021.147209, 2021.

Manisalidis, I., Stavropoulou, E., Stavropoulos, A., and Bezirtzoglou, E.: Environmental and Health Impacts of Air Pollution: A Review, Frontiers in Public Health, 8, https://doi.org/10.3389/fpubh.2020.00014, 2020.

Matsui, T., Zhang, S. Q., Lang, S. E., Tao, W. K., Ichoku, C., and Peters-Lidard, C. D.: Impact of radiation frequency, precipitation radiative forcing, and radiation column aggregation on convection-permitting West African monsoon simulations, Clim. Dyn., 55, 193-213, https://doi.org/10.1007/s00382-018-4187-2, 2018.

Mlawer, E. J., Taubman, S. J., Brown, P. D., Iacono, M. J., and Clough, S. A.: Radiative transfer for inhomogeneous atmospheres: RRTM, a validated correlated-k model for the longwave, J. Geophys. Res.-Atmos., 102, 16663-16682, https://doi.org/10.1029/97jd00237, 1997.

Molina, L. T., Madronich, S., Gaffney, J. S., Apel, E., de Foy, B., Fast, J., Ferrare, R., Herndon, S., Jimenez, J. L., Lamb, B., Osornio-Vargas, A. R., Russell, P., Schauer, J. J., Stevens, P. S., Volkamer, R., and Zavala, M.: An overview of the MILAGRO 2006 Campaign: Mexico City emissions and their transport and transformation, Atmos. Chem. Phys., 10, 8697-8760, https://doi.org/10.5194/acp-10-8697-2010, 2010.

Ning, G., Wang, S., Yim, S. H. L., Li, J., Hu, Y., Shang, Z., Wang, J., and Wang, J.: Impact of low-pressure systems on winter heavy air pollution in the northwest Sichuan Basin, China, Atmos. Chem. Phys., 18, 13601-13615, https://doi.org/10.5194/acp-18-13601-2018, 2018.

Pautasso, M., Dehnen-Schmutz, K., Holdenrieder, O., Pietravalle, S., Salama, N., Jeger, M. J., Lange, E., and Hehl-Lange, S.: Plant health and global change - some implications for landscape management, Biol. Rev., 85, 729-755, https://doi.org/10.1111/j.1469-185X.2010.00123.x, 2010.

Qian, Y., Chakraborty, T. C., Li, J., Li, D., He, C., Sarangi, C., Chen, F., Yang, X., and Leung, L. R.: Urbanization Impact on Regional Climate and Extreme Weather: Current Understanding, Uncertainties, and Future Research Directions, Adv Atmos Sci, 1-42, https://doi.org/10.1007/s00376-021-1371-9, 2022.

Ryu, Y. H., Baik, J. J., Kwak, K. H., Kim, S., and Moon, N.: Impacts of urban land-surface forcing on ozone air quality in the Seoul metropolitan area, Atmos. Chem. Phys., 13, 2177-2194, https://doi.org/10.5194/acp-13-2177-2013, 2013.

Schell, B., Ackermann, I. J., Hass, H., Binkowski, F. S., and Ebel, A.: Modeling the formation of secondary organic aerosol within a comprehensive air quality model system, J. Geophys. Res.-Atmos., 106, 28275-28293, https://doi.org/10.1029/2001jd000384, 2001.

Seto, K. C., Guneralp, B., and Hutyra, L. R.: Global forecasts of urban expansion to 2030 and direct impacts on biodiversity and carbon pools, Proc. Natl. Acad. Sci. U. S. A., 109, 16083-16088, https://doi.org/10.1073/pnas.1211658109, 2012.

Shu, Z., Liu, Y., Zhao, T., Xia, J., Wang, C., Cao, L., Wang, H., Zhang, L., Zheng, Y., Shen, L., Luo, L., and Li, Y.: Elevated 3D structures of $PM_{2.5}$ and impact of complex terrain-forcing circulations on heavy haze pollution over Sichuan Basin, China, Atmos. Chem. Phys., 21, 9253-9268, https://doi.org/10.5194/acp-21-9253-2021, 2021.

Song, Y., Wang, X., Maher, B. A., Li, F., Xu, C., Liu, X., Sun, X., and Zhang, Z.: The spatial-temporal characteristics and health impacts of ambient fine particulate matter in China, J. Clean Prod., 112, 1312-1318, https://doi.org/10.1016/j.jclepro.2015.05.006, 2015.

Stockwell, W. R., Middleton, P., Chang, J. S., and Tang, X. Y.: THE 2ND GENERATION REGIONAL ACID DEPOSITION MODEL CHEMICAL MECHANISM FOR REGIONAL AIR-QUALITY MODELING, J. Geophys. Res.-Atmos., 95, 16343-16367, https://doi.org/10.1029/JD095iD10p16343, 1990.

Tang, G. Q., Zhu, X. W., Xin, J. Y., Hu, B., Song, T., Sun, Y., Zhang, J. Q., Wang, L. L., Cheng, M. T., Chao, N., Kong, L. B., Li, X., and Wang, Y. S.: Modelling study of boundary-layer ozone over northern China - Part I: Ozone budget in summer, Atmos. Res., 187, 128-137, https://doi.org/10.1016/j.atmosres.2016.10.017, 2017.

Tewari, M., Chen, F., Wang, W., Dudhia, J., LeMone, M., Mitchell, K., Ek, M., Gayno, G., Wegiel, J., and Cuenca, R.: Implementation and verification of the unified NOAH land surface model in the WRF model, 20th conference on weather analysis and forecasting/16th conference on numerical weather prediction, 2165-2170.

UN DESA, 2018: World Urbanization Prospects: The 2018 Revision. United Nations Department of Economic and Social Affairs, Population Division.

Wang, H., Liu, Z., Wu, K., Qiu, J., Zhang, Y., Ye, B., and He, M.: Impact of Urbanization on Meteorology and Air Quality in Chengdu, a Basin City of Southwestern China, Frontiers in Ecology and Evolution, 10, https://doi.org/10.3389/fevo.2022.845801, 2022a.

Wang, H., Liu, Z., Zhang, Y., Yu, Z., and Chen, C.: Impact of different urban canopy models on air quality simulation in Chengdu, southwestern China, Atmospheric Environment, 267, https://doi.org/10.1016/j.atmosenv.2021.118775, 2021.

Wang, X., Chen, F., Wu, Z., Zhang, M., Tewari, M., Guenther, A., and Wiedinmyer, C.: Impacts of weather conditions modified by urban expansion on surface ozone: Comparison between the Pearl River Delta and Yangtze River Delta regions, Advances in Atmospheric Sciences, 26, 962-972, 2009.

Wang, Y., Yang, X., Wu, K., Mei, H., De Smedt, I., Wang, S., Fan, J., Lyu, S., and He, C.: Long-term trends of ozone and precursors from 2013 to 2020 in a megacity (Chengdu), China: Evidence of changing emissions and chemistry, Atmos. Res., 278, https://doi.org/10.1016/j.atmosres.2022.106309, 2022b.

Whiteman C D. Mountain meteorology: fundamentals and applications [M]. Oxford University Press, 2000.

Wu, K., Wang, Y., Qiao, Y., Liu, Y., Wang, S., Yang, X., Wang, H., Lu, Y., Zhang, X., and Lei, Y.: Drivers of 2013-2020 ozone trends in the Sichuan Basin, China: Impacts of meteorology and precursor emission changes, Environ Pollut, 300, 118914, https://doi.org/10.1016/j.envpol.2022.118914, 2022.

Yang, X., Wu, K., Wang, H., Liu, Y., Gu, S., Lu, Y., Zhang, X., Hu, Y., Ou, Y., Wang, S., and Wang, Z.: Summertime ozone pollution in Sichuan Basin, China: Meteorological conditions, sources and process analysis, Atmospheric Environment, 226, https://doi.org/10.1016/j.atmosenv.2020.117392, 2020.

Yin, P., Chen, R., Wang, L., Meng, X., Liu, C., Niu, Y., Lin, Z., Liu, Y., Liu, J., Qi, J., You, J., Zhou, M., and Kan, H.: Ambient Ozone Pollution and Daily Mortality: A Nationwide Study in 272 Chinese Cities, Environ Health Perspect, 125, 117006, https://doi.org/10.1289/EHP1849, 2017.

Yu, M., Carmichael, G. R., Zhu, T., and Cheng, Y.: Sensitivity of predicted pollutant levels to urbanization in China, Atmospheric Environment, 60, 544-554, https://doi.org/10.1016/j.atmosenv.2012.06.075, 2012.

Zardi, D. and Whiteman, C. D.: Diurnal Mountain Wind Systems, in Mountain weather research and forecasting, edited by: Chow, F. K., De Wekker, S. F. J., and Snyder, B., Springer, Berlin, 2013.

Zhan, C. and Xie, M.: Land use and anthropogenic heat modulate ozone by meteorology: a perspective from the Yangtze River Delta region, Atmos. Chem. Phys., 22, 1351-1371, https://doi.org/10.5194/acp-22-1351-2022, 2022.

Zhan, C., Xie, M., Liu, J., Wang, T., Xu, M., Chen, B., Li, S., Zhuang, B., and Li, M.: Surface Ozone in the Yangtze River Delta, China: A Synthesis of Basic Features, Meteorological Driving Factors, and Health Impacts, Journal of Geophysical Research: Atmospheres, 126, https://doi.org/10.1029/2020jd033600, 2021.

Zhan, C.-c., Xie, M., Fang, D.-x., Wang, T.-j., Wu, Z., Lu, H., Li, M.-m., Chen, P.-l., Zhuang, B.-l., Li, S., Zhang, Z.-q., Gao, D., Ren, J.-y., and Zhao, M.: Synoptic weather patterns and their impacts on regional particle pollution in the city cluster of the Sichuan Basin, China, Atmospheric Environment, 208, 34-47, https://doi.org/10.1016/j.atmosenv.2019.03.033, 2019.

Zhu, K. G., Xie, M., Wang, T. J., Cai, J. X., Li, S. B., and Feng, W.: A modeling study on the effect of urban land surface forcing to regional meteorology and air quality over South China, Atmospheric Environment, 152, 389-404, https://doi.org/10.1016/j.atmosenv.2016.12.053, 2017.